Contents

Chapter 5

C0 Interaction Region

5.1 Introduction

The goal of the C0 Interaction Region (IR) project is to produce high luminosity proton-antiproton collisions at the C0 region of the Tevatron for the BTeV experiment.

The key requirements for the IR design are:

- **Luminosity:** BTeV is designed to run at a peak luminosity of $2\times10^{32}\text{cm}^{-2}\text{s}^{-1}$. It is viewed as being competitive at half this luminosity. The starting point will be the luminosity achieved at the end of Collider Run 2 in 2009. The actual luminosity achievable in C0 is

$$\text{Luminosity (in CDF/D0 in 2009)} \times 35/\beta^*_{C0}\text{cm}. \tag{5.1}$$

  Thus, it is crucial to achieve the lowest possible β^* at C0. Based on our estimate of the success of machine upgrades, we have set the requirement that

$$\beta^*_{C0} \;<\; 50\,\text{cm} \tag{5.2}$$

- **Interoperability:** The C0 IR design must permit operation of the Tevatron for high luminosity at C0 or high luminosity at B0 and D0. Simultaneous operation of all three IRs at high luminosity is not a requirement. It is expected that this would require major changes to the Tevatron. With an appropriate lattice design, it will be possible to alternate between these two modes, B0/D0 and C0, to provide high luminosity collisions in all three areas in a time-shared manner, if desired. Simultaneous operation of C0 at high luminosity and one of the other areas at low luminosity is not a requirement of this design but is desirable and is expected to be possible.

- **Non-interference with BTeV Detector:** In order not to interfere with the BTeV detector, which is a "forward" spectrometer, IR components are required to be located outside of the C0 Collision Hall. Because of this requirement, the quadrupole closest to the IR will be approximately 5m farther away from the collision point than it is in B0 or D0. This adds to the challenge of achieving low β^*.

- **Schedule:** The IR components must be available for installation in the middle of FY09 to permit the lab maximal flexibility in scheduling the installation. The design should facilitate quick installation and commissioning, with a goal of doing this in 3-4 months.

- **Reuse of existing designs, components, and services:** To minimize the cost and technical risk of the project and to meet the relatively tight schedule, the design should take miximum advantage of existing components, designs, and infrastructure. R&D should be minimized.

- **Beam Crossing Time:** Although the current plan calls for operations with a 396 ns Bunch Crossing Interval, BTeV performance improves at 132 ns Bunch Crossing Interval. The design should not preclude operation at 132 ns.

- **Robustness:** The design must take maximum advantage of the information and operational experience that will be available about the Tevatron at the end of Run 2. This will minimize the commissioning time and improve the uptime.

The two largest technical components in the proposed design are modified LHC-style quadrupoles and newly designed corrector magnet packages (spools). This project takes full advantage of the Tevatron luminosity upgrades of the Run II Collider Program to obtain the highest luminosity possible for BTeV. It is designed to allow continued operation of the CDF and D0 experiments concurrently with the BTeV experiment. It makes use of proven existing Tevatron infrastructure to the fullest extent possible without compromising design goals. Modifications to the Tevatron are almost entirely restricted to the region from B43 to C17 (445 meters) and the 3 service buildings above.

The lattice design is robust. It utilizes asymmetric quadrupole triplets on either side of the IR to produce a 35 cm β^* at C0, the same design β^* as B0 and D0. Additional quadrupoles, some new and some reused from the Tevatron Low Beta Project, match to the Run II lattice at all energies and at all steps of the transition from injection to the low beta lattice. The C0 insertion itself introduces exactly one unit of tune to both horizontal and vertical planes, so that the Tevatron fractional tunes remain unchanged. This design minimizes the impact on Tevatron operation. Corrector magnet packages are designed to give excellent orbit control and coupling correction to provide added insurance against magnet misalignments and imperfections. The power supply configuration is versatile enough to tune out any foreseeable magnet errors. This lattice design is optimized for 36 x 36 bunch operation but does not preclude 132 nsec operation.

The LHC IR quadrupole produced by the Fermilab Technical Division is a well tested and proven magnet. A modification of this design provides a cost-effective and timely solution for the C0 IR project. The modifications are restricted to the cryostat and end enclosures of the magnet-the cold mass remains the same as the original LHC design.

The unique demands of the C0 IR and the antiquity of the original Tevatron spools preclude the use of these spools in this project. New spools will be designed and fabricated. The baseline design uses a standard nested cos(nθ) coil package to produce dipole, quadrupole,

and sextupole fields. In addition, these spools contain the high current leads for the low beta quadrupoles. Limitations in the helium liquifying capacity of the Tevatron cryogenic system necessitate the use of high temperature superconductor for these leads.

The scope of this project also encompasses the construction and installation of new power supplies, new cryogenic elements in the Tevatron tunnel, modifications to low conductivity water systems, vacuum systems, beam collimation systems, controls infrastructure, software, instrumentation, and operational procedures-all the things necessary to make a high energy accelerator function.

In the following sections of this chapter, we first describe the beam optics design that has been developed to meet these requirements; then, we provide a very brief discussion of the choice of the key technical components and the status of their development. Much more detail on the design may be found in the full conceptual design report [1] for the IR, from which the material presented in this chapter has been selected.

5.2 Accelerator Physics

5.2.1 Lattice

Every facet of successful Tevatron collider operations is tied intimately to specific details of the optical lattice functions in the ring. As examples, the locations of beam collimators, separators for helix generation, and the feeddown circuits are all determined largely by the distribution of betatron phase advance. So as not to disrupt these nominal Run II operating parameters it is essential that a new C0 Interaction Region (IR) insertion meld seamlessly with the existing Tevatron lattice. This implies the need to create an entirely localized insertion - one which is transparent to the rest of the machine. This constraint has important design implications, the most notable of which are pointed out below:

- An IR design similar to that employed at B0 and D0 is unacceptable as a C0 candidate. The addition of such a (single) low-β region to the machine would raise the tune by a half-integer in each plane, moving them far from the standard operating point and directly onto the 21.0 integer resonance. The nominal (fractional) tunes can be retained by adding 2 low-β's locally in each plane, thereby boosting the machine tunes by a full integer.

- The B0 and D0 IR's are not optically-isolated entities. Progression through the B0/D0 low-β squeeze involves adjusting, not only the main IR quadrupoles, but also the tune quad strings distributed around the ring. The result is that lattice functions at any point in the ring, and the phase advances across any section of the ring, are not fixed quantities, but vary through the squeeze sequence. For the operational mode of B0/D0-only collisions, the C0 insertion must be sufficiently flexible to track these changing matching conditions.

- With collisions only at B0 and D0 the unit of tune added by the C0 insert ensures that the incoming and outgoing helices are automatically matched into the Run II values. To maintain this match with collisions at all 3 IP's, however, would require additional separators in the short B0-C0 and C0-D0 arcs. There is no space available for more separators, so high luminosity collisions can only be created at B0 and D0, or just C0, but not all three simultaneously. Furthermore, without new arc separators the 2 IP collision options, B0 and C0 or D0 and C0, are also excluded.

Both the series and independent C0 IR quad circuits are illustrated in Figure 5.1. The specialized IR magnets required fall into 3 gradient ranges. First, there are LHC-like magnets operating at or just below 170 T/m. This is substantially less than the >220 T/m LHC design, but the gradients are limited here by the Tevatron 4.5^oK cryogenics. Second, there are high-field 140 T/m Q1 quadrupoles previously installed for Tevatron collider operation, but now no longer used. And third, there are strong (25 T.m/m) quad correction spools for the final optical match into the arcs.

The composition of the quadrupole circuits is described below, with the indicated lengths being magnetic lengths.

The triplet properties are:

quadrupole	length	Gradient
Q1	96.5"	170 T/m
Q2	173.5"	170 T/m
Q3	96.5"	170 T/m

Schematic layout of an IR triplet is given in Fig. 5.2, showing the slot lengths and magnetic lengths of the elements, and spaces allocated for flanges, cryo, coil supports, etc. A special correction package is installed between the Q2 and Q3 magnets. This contains both vertical and horizontal Beam Position Monitors(BPMs), dipole correctors in each plane, plus a trim skew quad. The dipole correctors are well situated for beam control at the IP: $\beta_x = \beta_y > 60\% \beta_{max}$, and the betatron phase advance to the IP is almost exactly 90^o in both planes. Because of the almost zero degrees of phase advance across the triplet magnets, the trim skew quad is perfectly located to compensate locally for triplet roll misalignments. The final focus triplets are powered in series, with a small additional power source added to Q2 for independent gradient variation to complete the match to the appropriate IP optics.

The properties of the quadrupoles at B48/C12 and B47/C13 are:

Quadrupole	length	gradient
Q4	79"	170 T/m
Q5	54"	170 T/m

Apart from their magnetic lengths the Q4 and Q5 magnets are the same design as the triplet quadrupoles, having adequate space at each end of the cryostat to accommodate the necessary ancillary hardware (see Fig. 5.2). These quadrupoles are accompanied by new, short (56.175") spools, containing BPM's and dipole correctors in each plane. These spools also serve as the magnet power feeds and transport the main bus.

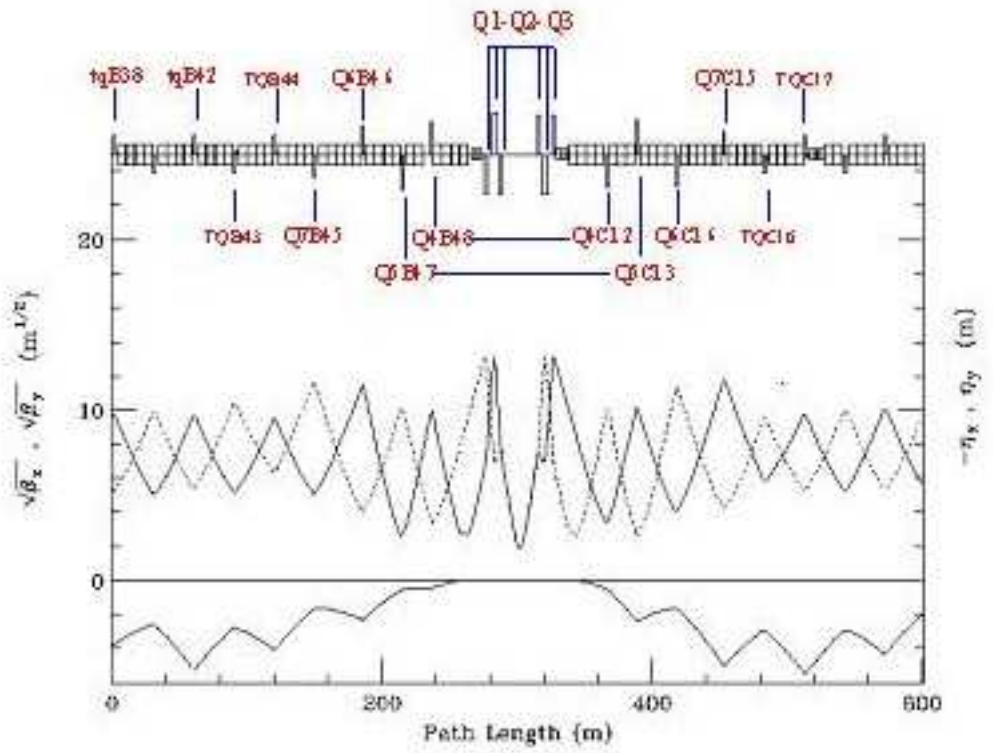

Figure 5.1: Power circuits of the IR quadrupoles

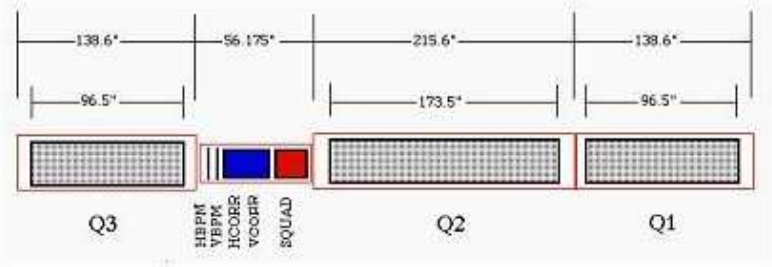

Figure 5.2: Details of the IR triplet

The properties of the quadrupoles at B46/B45 and C14/C15 are:

Quadrupole	length	gradient
Q6	55.19"	140 T/m
Q7	55.19"	140 T/m

The four Q6 and Q7 magnets are independently powered. The regular 66" arc quads and their spools at the B46, B45 (C14 and C15) locations are replaced with relocated high-field Q1 low-beta quads (defunct in Run II) from CDF and D0, along with their accompanying P spools. The P spools have BPM's and dipole correctors in each plane, plus a skew quad. These spools also serve as the magnet power feeds and transport the main bus.

There are spools at B43/B44 and C16/C17. The normal 72" Tevatron arc spools at these 4 locations are replaced by 72" spools containing high-field (25 T.m/m) trim quads plus standard strength horizontal or vertical dipoles and chromaticity sextupoles.

There are trim quadrupoles at B38 and B42. The trim quads (7.5 T.m/m) are removed from the main tune quad circuit and powered independently for final optical matching to the arc.

This design uses non-standard separations between some of the insertion's inner arc quadrupoles. Between the B48 and B47 (C12 and C13) quadrupole space is reduced by 1 dipole, whereas between B46 and B45 (C14 and C15) separation increases by 1 dipole. Extensive simulations have shown that this configuration contributes markedly to the robustness of the IR's tuning range.

Trim quads are allocated in a lopsided configuration, with 2 more installed in the upstream end of the insert. In B-sector it is possible to extend insert elements a good distance back into the arc before interfering with Run II operation. This is not so in C-sector. The 4 vertical separators at C17 are integral components of Run II operation, and therefore define the downstream insert boundary.

There are 15 optical constraints the insertion satisfies. The 6 incoming Twiss parameters are matched at the IP to

$$\beta_x^* = \beta_y^* = \beta^*,\ \alpha_x^* = \alpha_y^* = 0,\ \eta^* = 0,\ \eta'^* = 0 \tag{5.3}$$

and then matched back into the nominal arc values at the downstream end of the insert (at C17). The fractional Run II phase shifts, $\Delta\mu_x$ and $\Delta\mu_y$, are preserved across the insert. The final constraint imposed in the design is that $\beta_{x,max} = \beta_{y,max}$ in the triplets on each side of the IP. While this last restriction isn't really crucial, it is the best choice, minimizing the consumption of aperture in the low-β quads.

Every stage of the C0 low beta squeeze from $\beta^* = 3.50$ to 0.35m can match exactly to any step in the B0/D0 low beta squeeze. Subsequent sections illustrate these lattice parameters corresponding to the following specific operational conditions:

(1) Injection	β^*= 3.50 m at C0	(β_x^*,β_y^*) = (1.61,1.74) m at B0/D0
(2) C0 Collisions	β^*= 0.35 m at C0	(β_x^*,β_y^*) = (1.61,1.74) m at B0/D0
(3) B0/D0 Collisions	β^*= 3.50 m at C0	β^* = 0.35 m at B0 and D0

All gradient entries in the accompanying tables reflect 1 TeV/c operations.

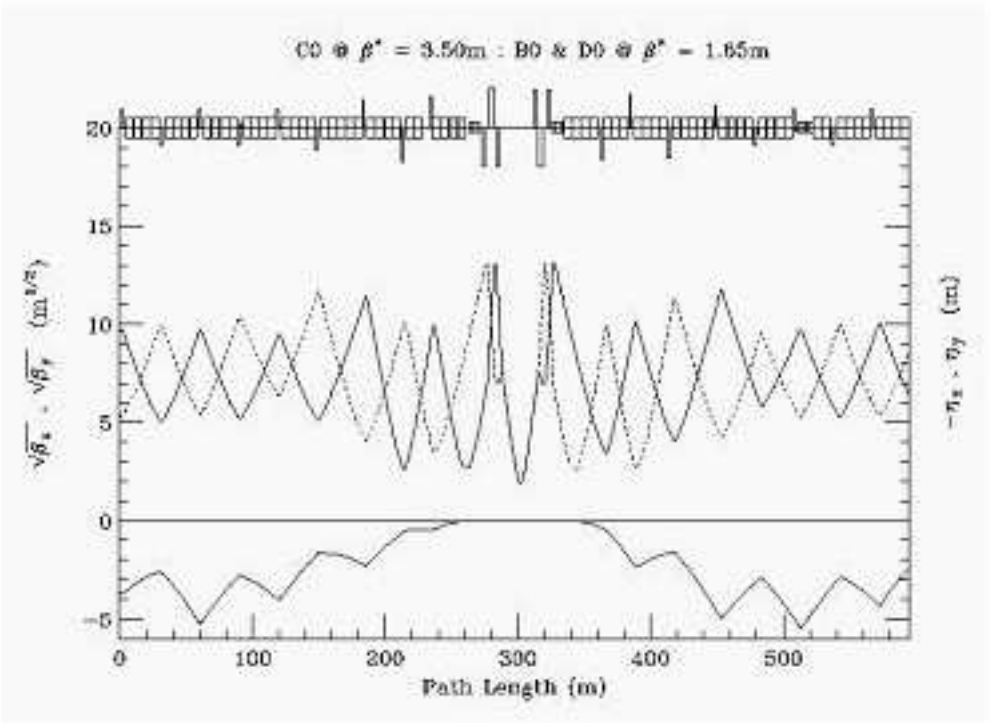

Figure 5.3: C0 injection optics

5.2.1.1 Injection

In the injection lattice, shown in Fig. 5.3, $\beta^* = 3.50$ m results in a β_{max} of 177 m in the triplets. This is appreciably less than the >240 m of the B0 and D0 injection lattices and, so, is not anticipated to pose any aperture problems for Tevatron operations. The corresponding quadrupole gradients are listed in Table 5.1 (at 1 TeV/c).

5.2.1.2 C0 Collisions

For collisions at C0, the B0 and D0 optics remain in their injection configuration, while at C0 β^* is squeezed from 3.50 m at injection to 0.35 m. Current Tevatron Collider understanding and experience suggests that the smallest realistic β^* attainable is limited by the adverse impact on the beam by high-order multipoles in the low-β quadrupoles and, therefore, β_{max} in the low beta triplets. In the C0 IR lattice the Q1 magnets at C0 are roughly 15' farther from the IP than the corresponding ones at B0 and D0. As a result, β_{max} is considerably larger at C0 for any given value of β^*. With $\beta^* = 35$ cm, β_{max} max has grown to 1660 m

INJECTION OPTICS: C0 $\beta^* = 3.50$m: B0/D0 $\beta^* = 1.65$m (1 TeV/c)					
	Gradient (T/m)	Current (A)		Gradient (T/m)	Current (A)
Q1D	-164.783	9267	Q1F	164.783	9267
Q2F	168.814	9493	Q2D	-168.814	9493
Q3D	-164.783	9267	Q3F	164.783	9267
QB48	133.019	7480	QC12	-133.019	7480
QB47	-145.047	8157	QC13	145.047	8157
QB46	117.055	4045	QC14	-122.786	4248
QB45	-92.551	3198	QC15	92.940	3211
TB44	4.939		TC16	-25.569	
TB43	17.724		TC17	-10.470	
TB42	6.793				
TB39	0				
TB38	3.013				

Table 5.1: C0 IR gradients for 1 TeV/c injection optics

(Figure 5.4), which is significantly larger than the β_{max} of ∼1130 m for a $\beta^* = 35$ cm at the other IP's. In addition, the 63 mm physical aperture of the LHC magnets is also less than the 70 mm of the B0/D0 triplets. Nonetheless, dynamic aperture studies indicate that this tighter aperture restriction should not be a limiting factor in determining the minimum β^* attainable.

For C0 collisions, β^* at the IP is squeezed to 35 cm - the same value as for B0/D0 collisions. The luminosity at C0 will therefore be identical to that of B0/D0 at the end of Run II. Anticipated Collider parameters at the end of Run II are summarized in Table 5.3.

5.2.2 B0/D0 Collisions

For collisions at just B0 and D0, the C0 β^* is fixed at its injection value of 3.50 m while at B0 and D0 β^* is squeezed from $\sim$ 1.65 m at injection to 0.35 m (see Figure 5.5). A comparison of C0 IR gradients listed in Table 5.4 with the injection values of Table 5.1 demonstrates the small tuning changes required at C0 to fix $\beta^* = 3.50$ m while maintaining the ideal optical match to the nominal Run II squeeze lattice.

5.2.3 Helix

With 36x36 bunch operation in the Tevatron there are 72 potential collision points of the proton and pbar beams. In Run II there are currently 6 sets of electrostatic separator modules available in both horizontal and vertical planes to keep the proton and pbar orbits separated everywhere in the ring except at the B0 and D0 IP's during collisions. One part of the Run II upgrade project is to increase by 5 the number of separator modules in the

C0 COLLISIONS $\beta^* = 0.35$m: B0/D0 $\beta^* = 1.65$m (1 TeV/c)					
	Gradient (T/m)	Current (A)		Gradient (T/m)	Current (A)
Q1D	-169.228	9517	Q1F	169.228	9517
Q2F	165.397	9301	Q2D	-165.397	9301
Q3D	-169.228	9517	Q3F	169.228	9517
QB48	169.688	9524	QC12	-169.688	9524
QB47	-168.875	9497	QC13	168.875	9497
QB46	91.625	3166	QC14	-101.950	3523
QB45	-66.539	2299	QC15	76.322	2637
TB44	9.528		TC16	-35.373	
TB43	-0.819		TC17	22.589	
TB42	-0.844				
TB39	0				
TB38	-7.424				

Table 5.2: C0 IR gradients for C0 collisions at β^*= 35 cm

C0 COLLISION PARAMETERS		
	Base Projection	Design Projection
protons/bunch	250	270×10^9
pbars/bunch	76.4	129.6×10^9
proton emittance	18	18 $\pi\mu$m
pbar emittance	18	18 $\pi\mu$m
β^* at C0 IP	0.35	0.35 m
Bunches	36	36
Bunch length(rms)	0.45	0.45 m
Hour-Glass Form Factor	0.70	0.70
Proton tune shift	0.005	0.008
Pbar tune shift	0.017	0.018
Initial Luminosity	160.5	294.0×10^{30}cm^{-2}s^{-1}

Table 5.3: Collider parameters projected for the end of Run II. The 'Base' projection uses conservative performance estimates for the Run II upgrade projects. The "Design" parameters include more ambitious, but realistic, expectations of the upgrades.

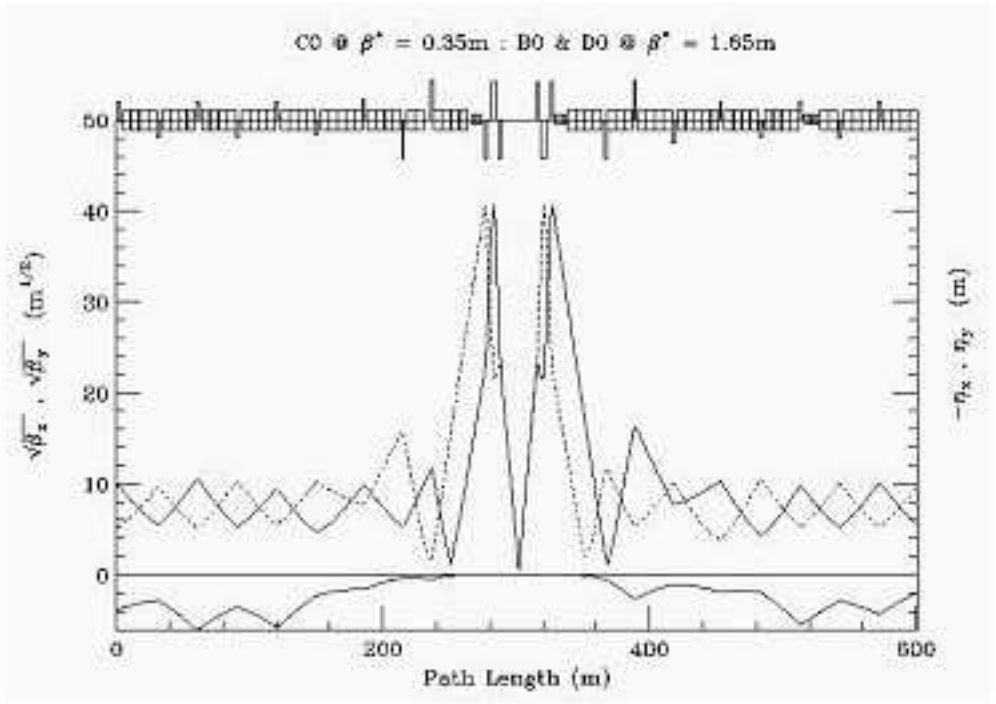

Figure 5.4: C0 collision optics - B38 to C19 (top) and ring-wide (bottom)

ring. The optimum sites for these new separators is still being studied. Another part of the Run II plan is to enhance the performance of the existing units. The present separators are run with gradients as high as ∼40 kV/cm (∼10.3 μrad kick at 1 TeV/c) before sparking becomes a problem. This is believed to be a conservative estimate of the maximum attainable gradient, however, and that with conditioning as much as a 30% increase should be possible. The outcome of these separator upgrades will be a better controlled, smoother helix at injection, where apertures are problematic, and increased beam separation at collision where the helix is limited by the available gradients. In view of the uncertainties still associated with implementing the Run II separator upgrade, however, in the discussions to follow only the currently installed ring separator configuration is considered, and the modules are assumed to have the conservative maximum electric field gradient of 40 kV/cm. In the BTeV era it is expected that the Tevatron will continue with 36x36 bunch operations. Additional separator modules will then need to be added to create collisions at the C0 IP. Like the other 2 IR's these will be installed immediately outboard of the C0 IR triplets. At B49 there will be a

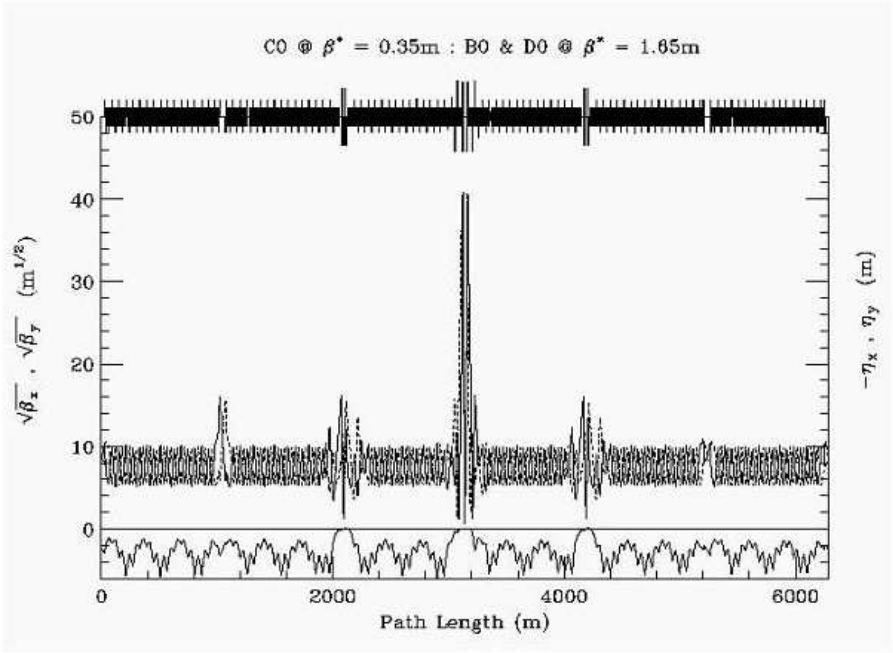

Figure 5.5: B0/D0 collision optics

B0/D0 COLLISIONS $\beta^* = 0.35$ m: C0 $\beta^* = 3.50$ m (1 TeV/c)					
	Gradient (T/m)	Current (A)		Gradient (T/m)	Current (A)
Q1D	-165.998	9335	Q1F	165.998	9335
Q2F	168.619	9482	Q2D	-168.619	9482
Q3D	-165.998	9335	Q3F	165.998	9335
QB48	131.721	7407	QC12	-131.721	7407
QB47	-144.299	8115	QC13	144.299	8115
QB46	117.055	4045	QC14	-122.786	4248
QB45	-92.551	3302	QC15	92.940	3211
TB44	8.059		TC16	-15.743	
TB43	9.440		TC17	-8.110	
TB42	6.252				
TB39	0				
TB38	3.870				

Table 5.4: C0 IR gradients for B0/D0 collisions and β^* fixed at 3.50 m at C0.

INJECTION HELIX: C0 $\beta^* = 3.50$m: B0/D0 $\beta^* = 3.50$m (150 GeV/c)					
Horizontal			Vertical		
	#	kV/cm		#	kV/cm
A49	1	0.0	A49	2	0.0
B11	2	-14.800	B11	1	-9.050
B17	4	25.740			
B49	2	0.0	B49	1	0.0
C11	1	0.0	C11	2	0.0
			C17	4	-26.150
C49	1	0.0	C49	2	0.0
D11	2	0.0	D11	1	0.0
D48	1	0.0			
			A17	1	0.0

Table 5.5: Injection Separator gradients at 150 GeV/c.

set of 2 horizontal modules and 1 vertical module, with the reverse configuration installed at C11.

5.2.3.1 Injection Helix

At the injection energy of 150 GeV, separation of the p-pbar orbits is controlled using a small subset of the 12 separators available in the machine. Separator strength is not an issue at 150 GeV, but the large beam sizes lead to aperture problems. The horizontal orbits are largely determined by the B17 separators, and the vertical by the C17 separators. The horizontal B17 gradients in particular are constrained by the aperture restrictions at the F0 injection Lambertson. One separator solution from Run II is listed in Table 5.5. Here, only 4 sets of separators are used to create the helix, and the new B49/C11 separators are not used at all. The resulting beam separation around the ring is shown in Figure 5.6. Outside of the B38-C17 C0 insert the helix is unchanged from the Run II value, and through the C0 IR region it can be seen that beam separation is at least as good as throughout the rest of the ring. The average separation is $\sim 8\sigma$.

5.2.4 C0 Collision Helix

For collisions at C0 the optics at B0 and D0 remain in their Injection configuration. In this case, all the separators in the ring become available for bringing beams together at the C0 IP, while keeping them separated everywhere else. One possible (minimal) separator solution is given in Table 5.6. The selection of separators has not been optimized particularly, other than to ensure adequate beam separation around the ring. Many more combinations still need to be explored.

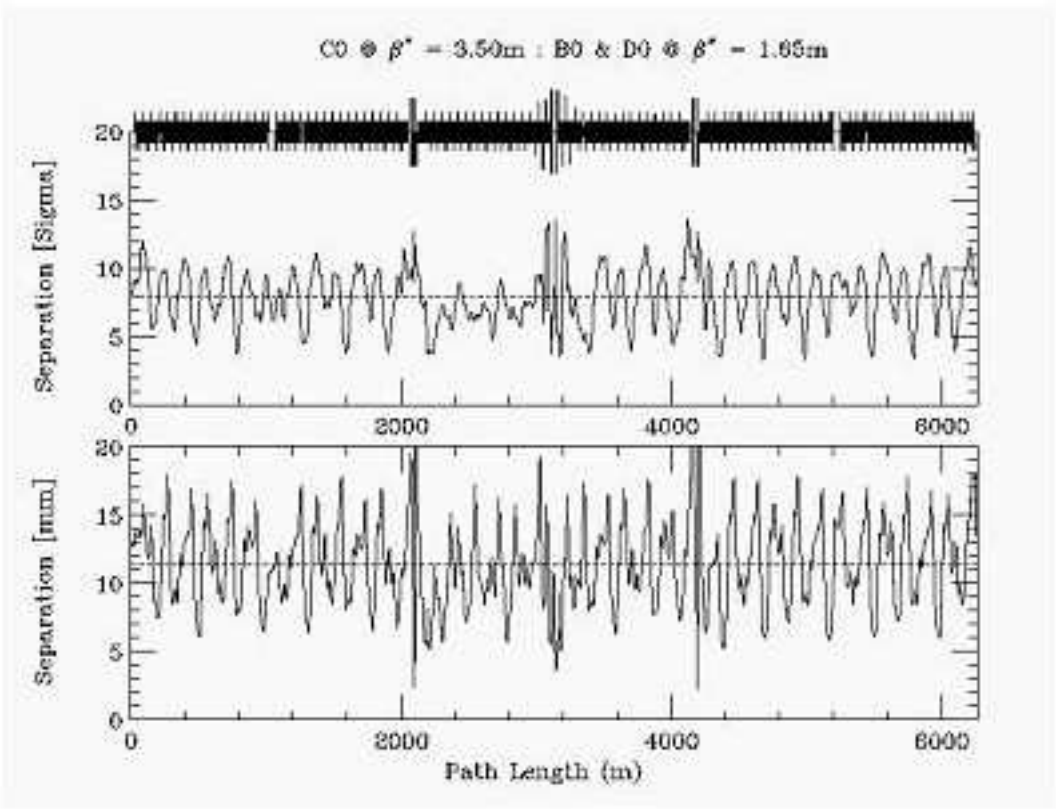

Figure 5.6: Injection helix at 150 GeV/c. $\epsilon_N = 20\pi$ μm and σ_p/p = 6×10^{-4}.

Figures 5.7 and 5.8 illustrate the beam separation around the ring and the separation across the insert from B38-C21,respectively. With this separator solution the closest approach through the insert is at the 1st parasitic crossing, where separation is about 3.7σ. Although 5σ separation is generally believed to be the minimum acceptable separation in the Run II collision lattice, dynamic aperture studies indicate that these 1st parasitic crossings are relatively benign for C0 collisions. Elsewhere in the ring, separation drops close to 5σ in a few spots, but otherwise the average separation is $\sim 8\sigma$. Oscillations in the helix could probably be smoothed further using a larger subset of separators.

5.2.5 B0/D0 Collision Helix

With collisions at just B0 and D0, the optics at C0 remain at the injection value of $\beta^* =$ 3.50 m, and the B49 and C11 separator voltages are turned up to create horizontal and vertical separation bumps at the C0 IP. Because the phase advance across the C0 separators is nearly 180^o in each plane, to a very good approximation the C0 bumps cancel away from the IR region. The settings of the rest of the ring separators remain essentially unchanged

C0 Collisions: C0 $\beta^* = 0.35$m: B0/D0 $\beta^* = 1.65$m (1 TeV/c)					
Horizontal			Vertical		
	#	kV/cm		#	kV/cm
A49	1	0.0	A49	2	25.744
B11	2	0.0	B11	1	-25.744
B17	4	18.112			
B49	2	-40.000	B49	1	-40.0
C11	1	40.000	C11	2	40.0
			C17	4	-20.355
C49	1	13.486	C49	2	0.0
D11	2	-13.486	D11	1	0.0
D48	1	0.0			
			A17	1	0..0

Table 5.6: C0 collision separator gradients at 1 TeV/c.

B0/D0 $\beta^* = 0.35$m: C0 $\beta^* = 3.50$m (1 TeV/c)					
Horizontal			Vertical		
	#	kV/cm		#	kV/cm
A49	1	40.000	A49	2	-33.287
B11	2	40.000	B11	1	40.000
B17	4	18.864			
B49	2	40.000	B49	1	40.0
C11	1	40.000	C11	2	40.0
			C17	4	-19.180
C49	1	37.197	C49	2	33.414
D11	2	-34.509	D11	1	40.0
D48	1	-5.162			
			A17	1	1.736

Table 5.7: Separator gradients for B0/D0 collisions at 1 TeV/c.

from their nominal Run II B0/D0 collision helix values (see Table 5.7). The resulting beam separation around the machine is shown in Figure 5.9 below. Away from the B0 and D0 IP's beam separation is $> 5\sigma$ everywhere, with an average separation of $\sim 8.5\sigma$.

5.2.6 Orbit Correction and Physical Aperture

From Table 5.8, dipole corrector bumps can be calculated for controlling position and angle at the IP. Tables 5.9 and 5.10 give the correct kick ratios for 2 efficient position bumps and 2 angle bumps in each plane. Other choices of magnet combinations are possible. The dipole

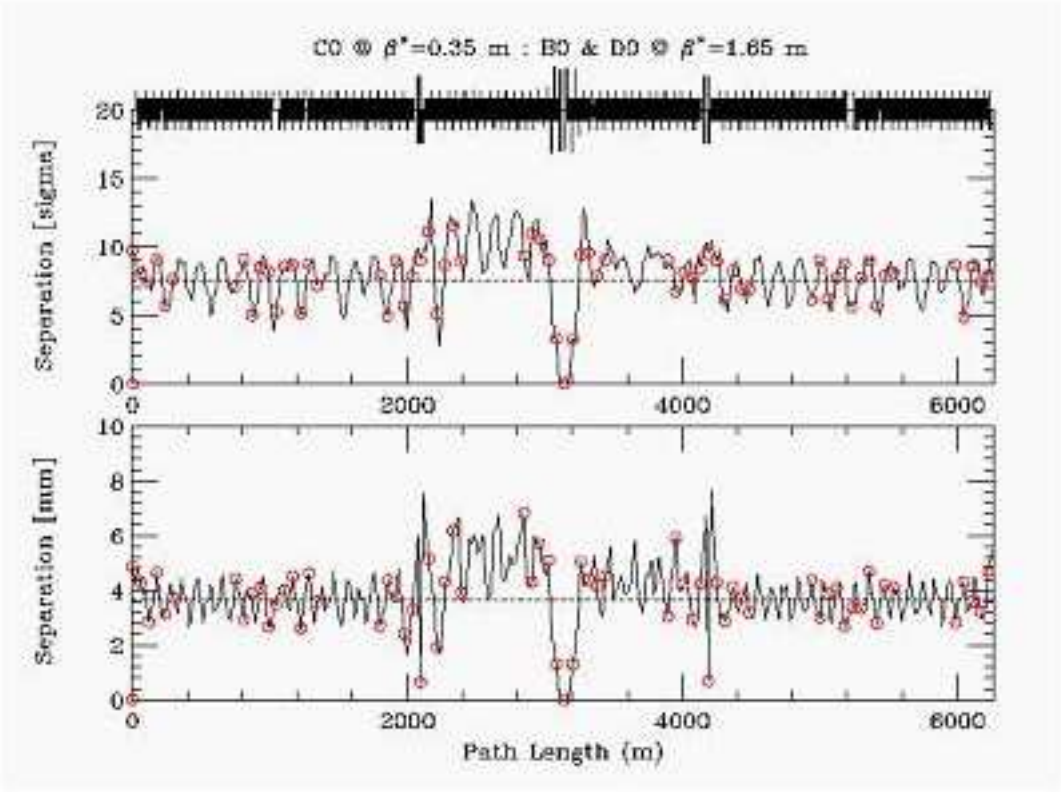

Figure 5.7: Beam separation around the ring during C0 collisions. $\epsilon_N = 20\pi\mu$m and σ_p/p = 1.47×10^{-4}.

correctors have integrated fields of 0.48 T.m. At 1 TeV/c this translates into a maximum kick angle of 144 μrad. Solutions (a) use the triplet spool package correctors, while solutions (b) use only arc correctors.

For position control at the IP the solutions (a), using the triplet correctors, are most effective. With $\beta_{corr} > 1000$m for $\beta^* = 0.35$ m, and with almost exactly 90^o of phase between the correctors and the IP, the beam position can be adjusted by as much as ±2.75 mm. This is nearly 3 times the control possible at the B0/D0 IR's. Furthermore, because there is nearly 180^o of phase separating the upstream and downstream packages the cancellation between the triplet corrector kicks is excellent, with very little orbit distortion leaking into the arcs for final elimination. The position bumps (b) use only arc spool packages. These would be useful either to supplement the triplet corrector solution, or to provide the IP position control in the event that the triplet dipoles are being used primarily to compensate for triplet quad misalignments. In any case, with the much smaller β-functions in the arc, solutions (b) are comparable to the orbit control at B0 and D0. At full corrector field the beam positions at the IP can be shifted by ±1.0 mm with solutions (b).

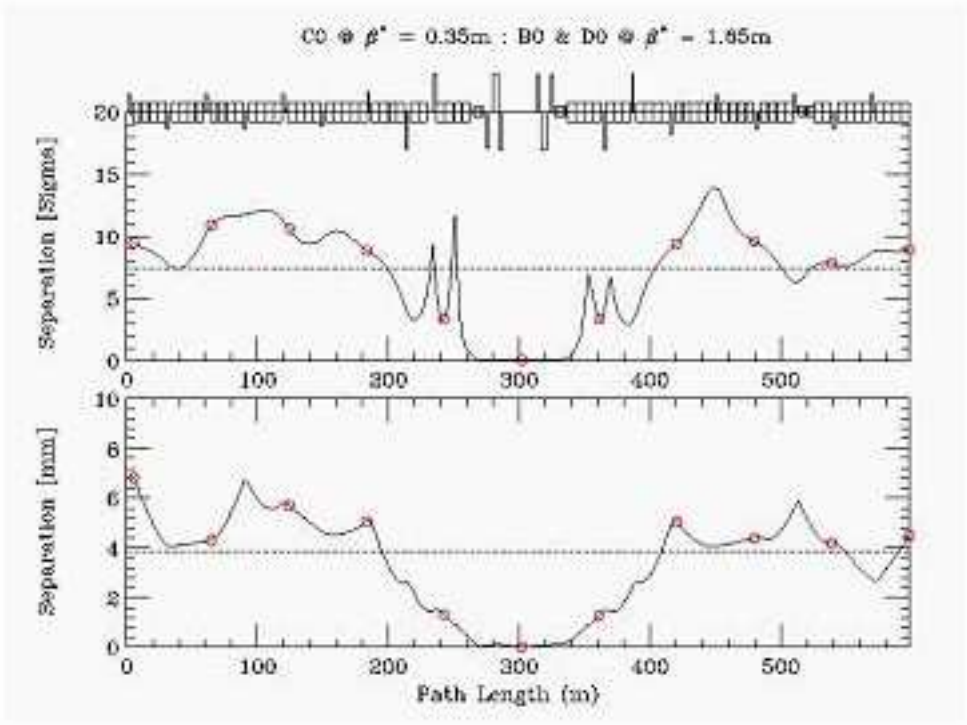

Figure 5.8: Beam separation through the insert during C0-only collisions. $\epsilon_N = 20\pi\mu$m and $\sigma_p/\mathrm{p} = 1.47\times10^{-4}$.

For angle control at the IP there is no overpowering reason to prefer one of solutions (c) or (d) over the other. In either case the IP angle must be generated out in the arcs and the level of angle control possible at the IP is limited by the aperture in the low beta triplet quadrupoles rather than the available field strengths of the correction dipoles. For a $20\pi\mu$m beam at 1 TeV, and $\beta_{max} = 1660$ m in the triplets, the 1σ beam width is $\sim$2.5 mm. The quadrupole physical aperture has a radius of only 31.5 mm. In an extremely optimistic scenario which imagines the beam orbit can be displaced by as much as 25 mm in the triplet quadrupoles, the corresponding angle control at the IP is $\pm$1.04 mrad.

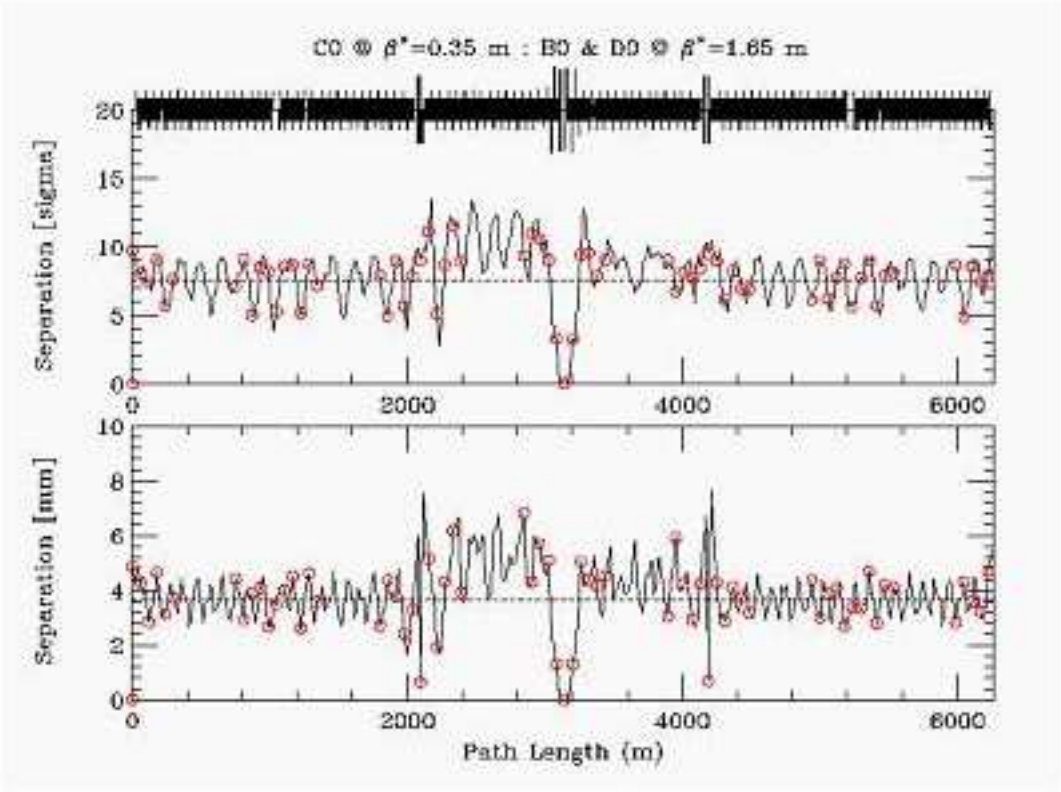

Figure 5.9: Separation during B0 and D0 collisions. $\epsilon_N = 20\pi\mu$m and σ_p/p = 1.47×10^{-4}.

5.2.7 Higher Order Correction

5.2.7.1 Quadrupole Misalignment

The effects of misaligned quadrupoles other than the triplet quadrupoles are straightforward to correct using the arc correction spools between B38 and C17 listed in Table 5.8. The following discussion therefore is limited to the triplets.

Two types of misalignment are particularly harmful - transverse misalignments, which deliver kicks to the beam, and roll of the quadrupoles about the longitudinal axis, leading to coupling of the two transverse planes. The beam optics are not as sensitive to other misalignments, such as displacement of the magnets along their longitudinal axis. Transverse misalignments can be corrected using the position bumps described in the preceding section. With maximum integrated fields of 0.48 T.m, the triplet spool correction dipoles can compensate for systematic transverse displacements of the triplet by ±0.5 mm, and random transverse errors of ±0.25 mm.

Rolls of the triplet quadrupoles introduce coupling that degrades luminosity. Although

C0 IR CORRECTION SPOOL PACKAGES							
Site	Spool Type	Elements	β_x (m)	μ_x (2π)	η_x (m)	β_y (m)	μ_y (2π)
B38	TSE	HD, QTF, SxF	90.4	0.005	3.66	29.6	0.018
B39	TSB	VD, QTD, SxD	33.2	0.104	3.00	87.2	0.110
B42	TSC	HD, QTF, SxF	103.6	0.182	5.87	30.0	0.217
B43	X1	VD, QT, SxD	29.8	0.278	3.57	100.2	0.301
B44	X1	HD, QT, SxF	84.6	0.371	5.54	32.3	0.395
B45	TSP	H&VD, SQ, H&VBPM	23.1	0.491	2.22	102.7	0.476
B46	TSP	H&VD, SQ, H&VBPM	92.9	0.622	1.48	66.6	0.552
B47	X2	H&VD, H&VBPM	33.4	0.723	0.32	210.6	0.588
B48	X2	H&VD, H&VBPM	123.8	0.767	0.43	1.70	0.777
B49	TSH	H&VD, SQ, VBPM	160.7	1.240	0.00	875.0	1.047
C0 U	X3	H&VD, SQ, H&VBPM	1042.	1.247	0.00	1017.	1.049
C0*			0.35	1.494	0.00	0.35	1.297
C0 D	X3	H&VD, SQ, H&VBPM	1017.	1.742	0.00	1042.	1.545
C12	X2	H&VD, H&VBPM	17.3	1.778	0.43	95.4	2.018
C13	X2	H&VD, H&VBPM	253.4	2.207	2.53	30.6	2.087
C14	TSP	H&VD, SQ, H&VBPM	59.9	2.247	1.03	95.7	2.171
C15	TSP	H&VD, SQ, H&VBPM	99.0	2.320	1.88	17.0	2.356
C16	X1	VD, QT, SxD	20.6	2.447	2.08	104.1	2.474
C17	X1	HD, QT, SxF	90.1	2.558	5.32	29.7	2.571

Table 5.8: C0 IR correctors and lattice functions. Here HBPM and VBPM are horizontal and vertical position monitors; HD and VD are trim dipoles (0.48 T.m); QTF and QTD are tune quads (7.5 T.m/m); SxF and SxD are chromaticity sextupoles (450 T.m/m^2); QT are strong trim quadrupoles (25 T.m/m); and SQ are skew quadrupoles (7.5 T.m/m)

this coupling can be corrected globally with distributed skew quadrupoles, reduction in luminosity is unavoidable unless there are skew correction elements located physically at the triplets. Table 5.11 lists the locations of skew quadrupoles, and their contributions to the real and imaginary components of the coupling coefficient. Because there is essentially zero phase advance across the triplets it can be seen that the triplet skew quad elements at C0U and C0D are ideally situated to correct for roll errors of the triplet magnets.

To estimate the integrated skew gradient of the triplets, 1000 random cases have been studied with all six quadrupoles rolled independently. With uniformly distributed rolls between $\pm\Phi$, the real and imaginary parts of the integrated skew gradients (when multiplied by $\sqrt{\beta_x\beta_y}$) are 980 and 2835Φ T.m, respectively (with Φ in mrad). The maximum integrated field of the C0U and C0D skew quadrupoles is 7.5 T.m/m, so that the triplet correctors are capable of compensating locally for random roll angles Φ as large as 2.5 mrad. For larger roll

	X^* POSITION BUMP COEFFICIENTS		**Y^* POSITION BUMP** COEFFICIENTS	
	(a)	(b)	(a)	(b)
B45			-0.0706	-0.0052
B46	-0.0861	+0.5043		
B47				
B48				
B49		1.0 θ		-0.3881
C0U	+0.9882		1.0 θ	
C0	$X^* = 19.1\theta$	7.3θ	$Y^* = 18.4\theta$	6.8θ
C0D	$+1.0\theta$		+0.9043	
C12				1.0θ
C13		-0.5461		
C14			-0.0818	+0.2622
C15	-0.0686	-0.4359		

Table 5.9: Relative dipole kick strengths to vary the beam positions (x^*, y^*) at the IP while fixing the angles (x'^*, y'^*)= 0. Positions (x^*, y^*) are in mm and θ is corrector the kick angle in mrad of the strongest corrector.

	X'^* ANGLE BUMP COEFFICIENTS		Y'^* ANGLE BUMP COEFFICIENTS	
	(c)	(d)	(c)	(d)
B45			1.0 θ	1.0 θ
B46	-0.6812	+0.8620		
B47				
B48		-0.5443		
B49				
C0U	-0.1467		0.3003	
C0	$X'^* = 7.8\theta$	11.2θ	$Y'^* = 7.6\theta$	11.4θ
C0D	0.2772		-0.1336	
C12				0.6029
C13		0.5708		
C14			0.6419	-0.8284
C15	1.0 θ	1.0 θ		

Table 5.10: Relative dipole kick strengths to vary the angles (x'^*, y'^*) at the IP while fixing the beam positions (x^*, y^*)=0. Angles (x'^*, y'^*) are in rad and θ is corrector kick angle in rad of the strongest corrector.

SKEW QUAD CORRECTORS FOR TRIPLET ROLL MISALIGNMENTS					
Spool	β_x (m)	β_y (m)	$2\pi\,(\mu x - \mu y)$ (deg)	$\sqrt{\beta_x\beta_y}\cdot\cos(\Delta\mu)$ (m)	$\sqrt{\beta_x\beta_y}\cdot\sin(\Delta\mu)$ (m)
PACKB45	23.1	102.7	5.4	48.49	4.58
PACKB46	92.9	66.6	25.2	71.17	33.49
PACKB49	160.7	875.0	69.5	131.32	351.24
Q3D	570.0	1593.	70.9	311.75	900.28
PACKC0U	1042.	1017.	71.3	330.05	975.08
Q2F	1660.	467.9	70.9	288.44	832.96
Q1D	619.5	538.0	70.9	188.90	545.50
Q1F	538.0	619.5	70.6	191.75	544.50
Q2D	467.9	1660.	71.3	282.62	834.95
PACKC0D	1017.	1042.	70.9	336.84	972.75
Q3F	1593.	570.0	71.3	305.46	902.43
PACKC14	59.9	95.7	27.4	67.22	34.84
PACKC15	99.0	17.0	-13.0	39.97	-9.23

Table 5.11: Skew quadrupole locations and their real and imaginary coupling components. The midpoint optics values of the Q1, Q2, and Q3 IR magnets are also given.

misalignments the B49 corrector is useful for global compensation, and the B45, B46, and C14, C15 correctors can be used to fine tune cancellation of the real coupling component.

5.2.8 Feeddown Circuits

The Tevatron sextupole and skew sextupole circuits are used to adjust the tunes and coupling of the protons and pbars independently during collider operation. In particular, these circuits can adjust the difference in horizontal and vertical tunes, and sine and cosine components of the coupling between the proton and pbar helices. The 7 feeddown families and their functionality in Run II are listed in Table 5.12. Four of the families are used for the injection helix and another set of four is used for the B0/D0 collision helix. (The S1 family is shared.) The family elements are given in Table 5.13.

When the beams travel off-axis through the sextupoles, they see feeddown normal and skew quadrupoles, the effects of which depend on the orientation of the helix, and the polarity and tilt angle of the magnet. Installation of the C0 interaction region will eliminate the 2 skew sextupoles at B43 and B47 from the S2 family. The S2 family is used for adjusting the differential vertical tune, and is used only with the injection helix. Two possibilities are currently being explored to compensate for the missing elements: (i) Since there will still be 10 S2 elements distributed in the ring, it might be acceptable simply to increase the S2 circuit current by $\sim$20%; (ii) It should be possible to move these 2 elements to other locations in the

Circuit	Injection Helix	Collision Helix
S1	$\Delta\nu_x$	ΔC_{sq}
S2	$\Delta\nu_y$	
S3	ΔC_{sq}	
S4		$\Delta\nu_x$
S5		$\Delta\nu_y$
S6	ΔS_{sq}	
S7		ΔS_{sq}

Table 5.12: Feeddown circuits and their functionality: $\Delta\nu_x$, $\Delta\nu_y$ are the differential tunes; ΔC_{sq}, ΔS_{sq} are the cosine and sine components of the differential coupling.

ring which have the appropriate helix orientation and lattice functions. Example replacement sites are listed in Table 5.14 below.

5.2.9 Dynamic Aperture Calculations

Realistic tune footprint and dynamic aperture calculations require the inclusion of lattice nonlinearities. The studies described below include the B0/D0 IR triplet quadrupole multipoles, chromatic sextupoles, and the multipoles of the C0 LHC triplet magnets. The LHC multipoles are listed in Table 5.15. All calculations correspond to the top energy of 980 GeV for C0 collisions at $\beta^* = 35$ cm on the collision helix.

5.2.9.1 Single Beam

The single beam tune footprint can be a good measure of the impact of the machine nonlinearities on the beam. Figure 5.10 shows the tune footprint extending to amplitudes of 6σ in each plane. Without the C0 triplet magnet errors the horizontal tune spread is twice the vertical spread at $(\Delta\nu_x, \Delta\nu_y) = (8\times10^{-5}, 4\times10^{-5})$. The inclusion of the C0 IR errors does not greatly affect the tune spreads; $(\Delta\nu_x, \Delta\nu_y) = (8\times10^{-5}, 6\times10^{-5})$(Fig. 5.11) , but the shape of the distribution is appreciably altered. For comparison, the corresponding tune footprint in the current Run II Tevatron lattice with B0/D0 collisions is shown in Figure 5.12. The Run II B0/D0 lattice tune spread is approximately 6×10^{-4} in both planes - a factor of 10 or more broader than in the C0 collision lattice.

The dynamic aperture is calculated by launching particles at several angles in x-y space. In the following calculations 13 launch points were taken, spaced apart by 7.5^o from 0^o (horizontal) to 90^o (vertical). The radial dynamic aperture at each angle is then calculated to be the largest stable amplitude below which all amplitudes are stable. A comparison of the single beam dynamic aperture with the dynamic aperture including beam-beam forces indicates the relative importance of beam-beam effects. Figure 5.13 shows the calculated single beam dynamic aperture for C0 collisions averaged over 5 seeds for the magnetic multipoles.

Circuit Name	Polarity	Magnet location	Spool type	Circuit Name	Polarity	Magnet location	Spool type
C:S1B1A	-	B19	E	C:S3A2A	+	A17	C
C:S1B3A	+	B38	E		-	A24	C
C:S1C2A	+	C24	E	C:S3D2A	-	D19	C
	-	C32	G		+	D26	C
C:S1E2A	+	E24	E	C:S3D4A	+	D38	C
	-	E28	E		-	D46	C
C:S1F2A	+	F19	E	C:S3E1A	-	E17	C
	-	F26	G		+	E22	C
C:S1F3A	+	F34	E	C:S3E3A	-	E32	C
	-	F38	E		+	E36	C
C:S2A1A	-	A14	D	C:S4C2A	+	C19	E
C:S2A3A	+	A33	D		-	C26	G
C:S2B4A	-	B43	D	C:S4C2B	+	C22	G
	+	B47	D		-	C28	E
C:S2C3A	+	C27	D	C:S4F2A	+	F24	E
	-	C33	D		-	F28	E
C:S2D2A	-	D23	D	C:S5A2A	+	A18	D
	+	D27	D	C:S5A3A	-	A37	D
C:S2F1A	+	F12	D	C:S5D3A	-	D33	D
	-	F16	D		+	D37	D
C:S2F2A	+	F23	D	C:S5F1A	-	F14	D
C:S2F4A	-	F43	D	C:S5F3A	+	F33	D
				C:S6A4A	+	A46	T:SF
				C:S6C4A	-	C46	T:SF
				C:S7B1A	+	B14	T:SD
				C:S7D1A	+	D14	T:SD

Table 5.13: Locations, magnet elements, and polarities of the 7 feeddown family members. Note that spool types TSC and TSD contain skew sextupoles – all others contain normal sextupoles.

The maximum separation launched was 25σ. The average dynamic aperture is 24σ - well beyond the physical aperture of the low-β quads. From Figure 5.14 it can be seen that this C0 collision lattice average dynamic aperture is nearly twice as large as the single beam dynamic aperture calculated for Run II B0/D0 collisions. In that case, also calculated for $\Delta p/p = 3\times10^{-4}$, the average dynamic aperture is just 12.3σ.

Site	Spool	β_x (m)	β_y (m)	$\mu_x - \mu_y$ (deg^o)	X_o (mm)	Y_o (mm)
B43	TSD	32.7	95.4	26.6	-0.50	-5.20
D43	TSD	33.1	94.9	30.8	+0.66	+5.76
E43	TSF	33.2	93.9	29.2	-0.67	-5.86
B47	TSD	30.5	89.8	28.1	+3.62	+4.02
E27	TSFR	30.7	93.2	28.1	+3.73	+6.39
E47	TSFR	30.5	92.8	25.5	-4.08	-6.01

Table 5.14: Possible locations in the ring where the B43 and B47 skew sextupole S2 circuit elements could be relocated.

LHC HARMONICS 11922 A					
	Average	Sigma		Average	Sigma
b3	0.31	0.47	a3	-0.57	0.65
b4	0.02	0.48	a4	0.30	0.39
b5	-0.03	0.13	a5	-0.38	0.18
b6	-0.02	0.45	a6	-0.04	0.11
b7	-0.01	0.03	a7	0.01	0.03
b8	0.00	0.02	a8	0.01	0.03
b9	0.03	0.01	a9	-0.02	0.03
b10	0.01	0.02	a10	-0.03	0.02

Table 5.15: LHC quadrupole magnetic nonlinearities included in dynamic aperture studies.LHC HARMONICS at 11922 A. LHC harmonics reported in "units" at a reference radius of 17 mm. Harmonics are a weighted average over body + end fields for 6 magnets. All data was taken at 215 T/m.

5.2.9.2 Beam-beam

With 36x36 operation there are 71 long-range interactions between the separated proton and pbar bunches in addition to the head-on collision at the C0 IP. The long-range interactions are more complex than the head-on collisions. In addition to changing the tunes, these parasitic interactions also change the orbits, coupling, and chromaticity.

The tune footprint for pbar bunch #6 is shown in Figure 5.15., including the beam-beam forces in addition to the magnetic nonlinearities discussed earlier. The tune spread has grown by about 2 orders of magnitude compared to the single beam analysis, to ($\Delta\nu_x$,$\Delta\nu_y$) = (8×10^{-3}, 9×10^{-3}). This spread is still a factor of 3 less than the corresponding footprint for the Run II B0/D0 collision lattice, as given in Figure 5.16. In the Run II lattice the spread is approximately equal in both planes at $\Delta\nu = 2.3\times10^{-3}$. In both of these cases most of the contribution comes, not from the head-on collisions, but from the 1st parasitic crossings on each side of the IP. While the beam separation at the C0 first parasitics is $\sim3.7\sigma$, or about

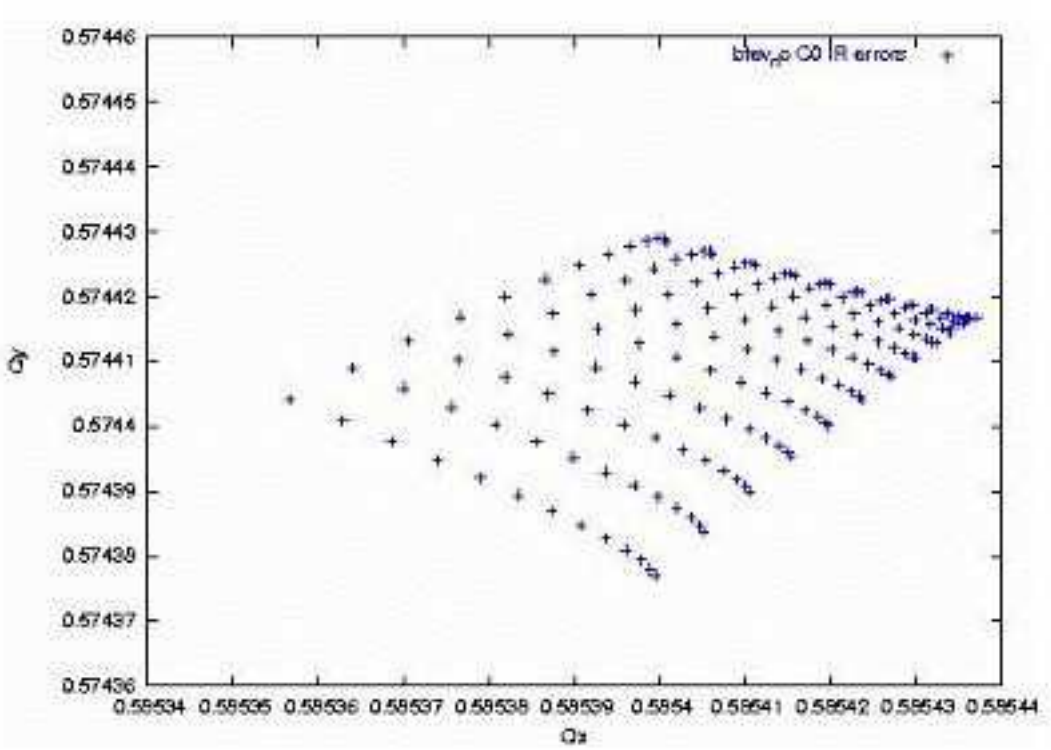

Figure 5.10: Single beam tune footprint, in the absence of C0 IR quadrupole errors. The base tunes are (.585, .575).

half the separations at B0 and D0's nearest misses in Run II, this is compensated to a large extent by there being only one IP and two nearest miss points, as compared to the two IP's and four nearest misses of Run II.

Figure 5.17a shows the dynamic aperture including beam-beam effects for C0 collisions, averaged over the magnetic multipoles generated by 5 seeds. The average dynamic aperture is 14σ, indicating that beam-beam effects reduce the aperture of the machine by a substantial 10σ. However, this analysis also suggests that the minimum dynamic aperture of 12σ should exceed the physical aperture set by the primary collimators, which are typically placed at $\sim 6\sigma$. By comparison with Figure 5.17b it can be seen that the average dynamic aperture in the C0 collision lattice is roughly twice as large as the 8σ average calculated for Run II B0/D0 collisions, and, furthermore, the C0 *minimum* dynamic aperture of 12σ even significantly exceeds the *maximum* 9σ dynamic aperture of the Run II lattice.

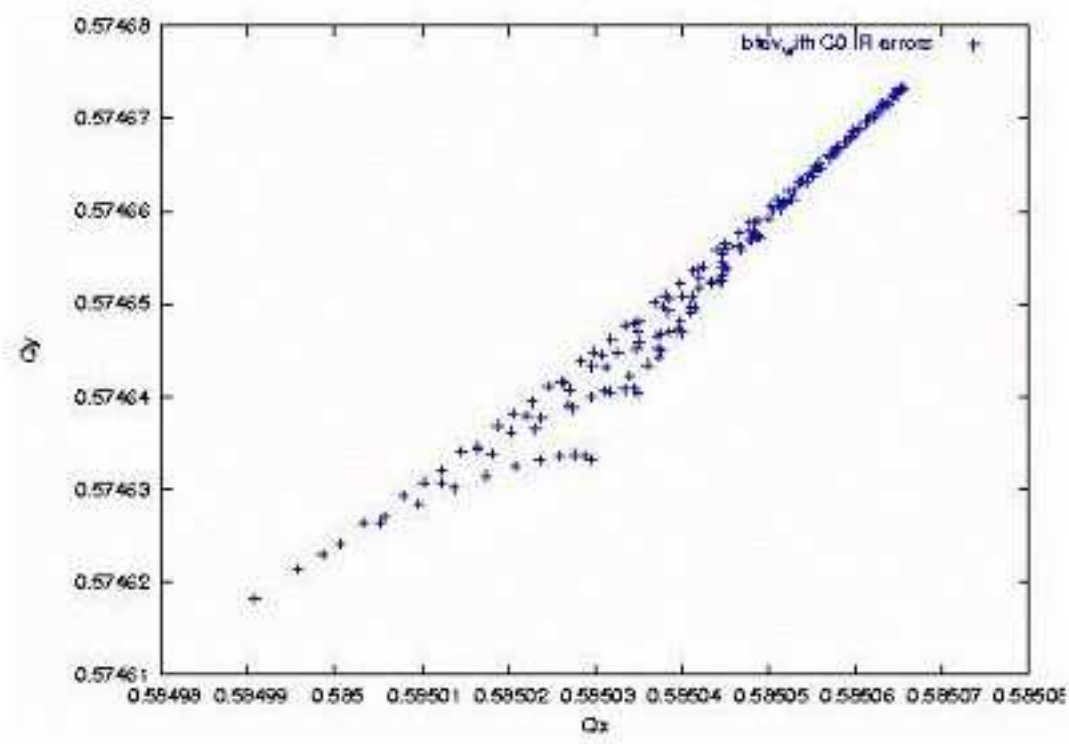

Figure 5.11: Tune footprint of a single beam in the C0 lattice, with LHC quad harmonics, with collisions at B0 and D0.

5.3 Key Technical Details

The implementation of the design described above for a new insertion in the Tevatron to produce high luminosity collisions at C0 is highly constrained by the amount of space available and the existing technical components. Basing the design on existing components wherever possible is crucial to its timely and cost effective implementation. R&D programs for technical components with these demanding specifications are expensive, time consuming, and there is no assurance that they will succeed. Modifying existing designs and building on past experience with similar projects is a key to insuring success.

5.3.1 LHC Style Quadrupoles - Overview and Conceptual Design

The C0 IR described above requires quadrupoles of a new design for the Q1 through Q5 magnets. Table 5.16 shows the locations, gradient, magnetic length and mechanical slot length requirements of these elements. The nominal operating temperature is 4.5K.

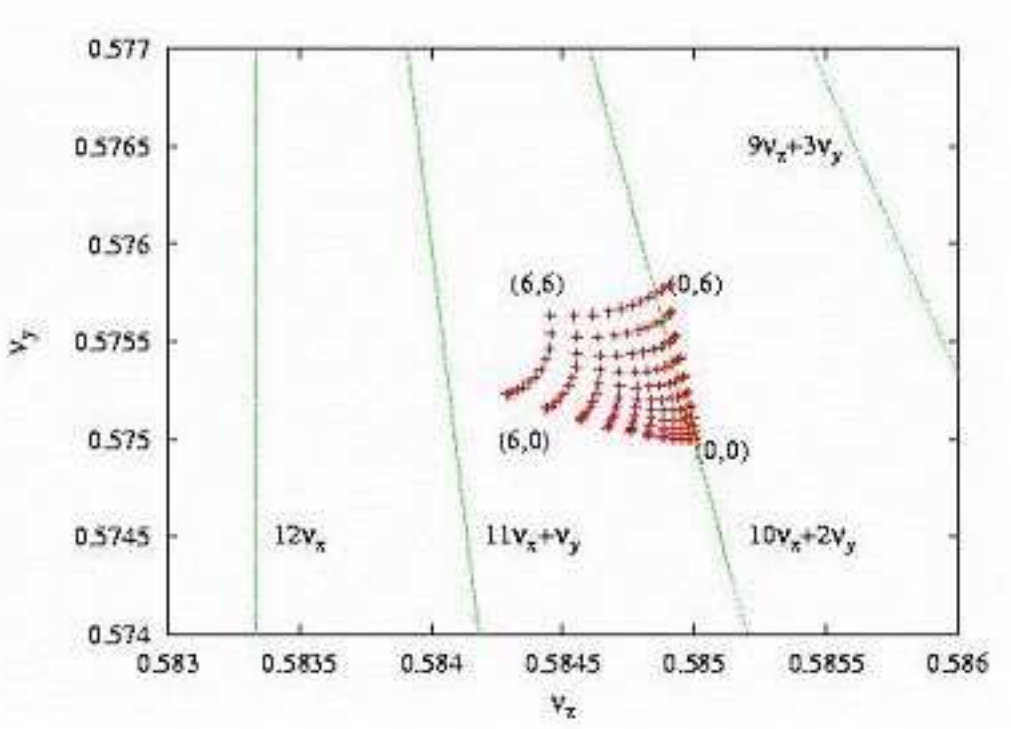

Figure 5.12: Single beam dynamic aperture forthe current Run II lattice with $\epsilon_N = 20\pi\mu$m and Δp/p = 3×10^{-4}.

Magnet	Nominal Gradient	Magnetic Length	Magnetic Center	Mechanical Slot Length
	(T/m)	(m)	(m from IP)	(m)
Q1	169.2	2.41	14.263	3.520
Q2	165.4	4.43	18.749	5.476
Q3	169.2	2.41	24.661	3.520
Q4	170.0	2.01	65.115	2.974
Q5	170.0	1.37	86.911	2.441

Table 5.16: Q1 - Q5 Parameters

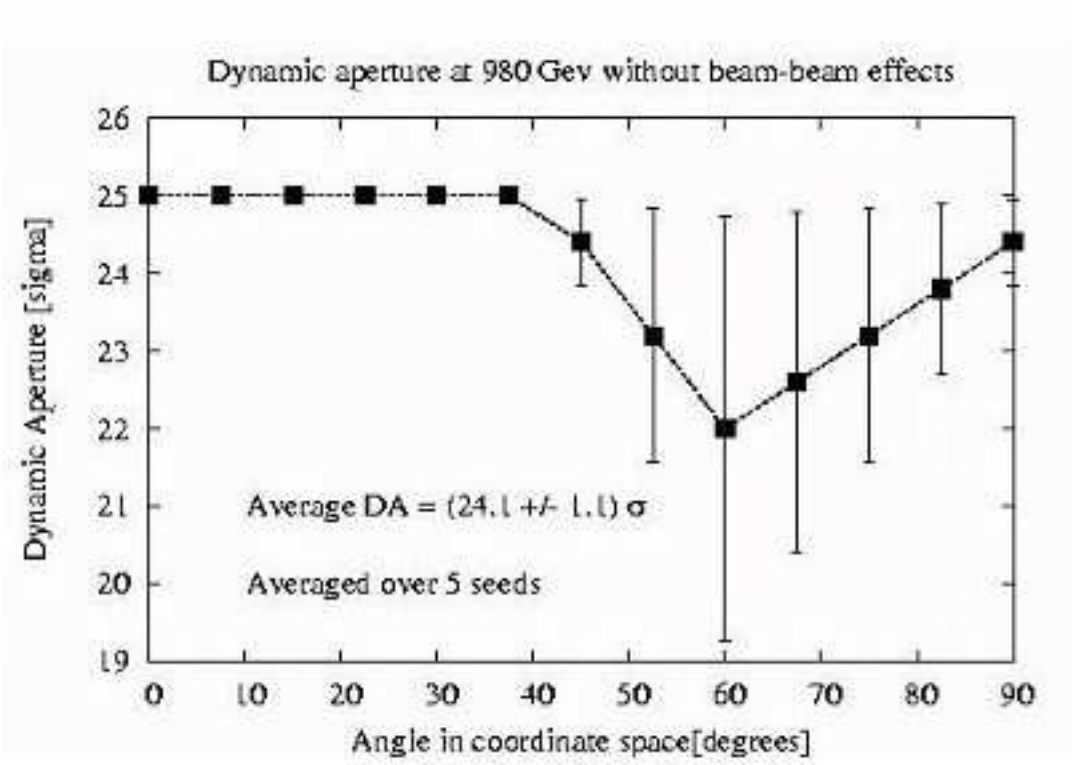

Figure 5.13: C0 collision lattice. Single beam dynamic aperture with $\epsilon_N = 20\pi\mu$m and Δp/p $= 3\times10^{-4}$.

To meet these requirements, we propose a design based on the collared coil assembly of the well proven LHC IR quadrupole currently in production, with the magnet length, iron yoke, cryostat, cryogenic system, and interconnects re-optimized for the C0 IR. Figure 5.18. shows a cross-section of the collared coil of such a magnet.

The coil bore is 70mm, which allows for use of a beam tube with inside diameter 63mm. The reuse of the body design of the LHC quadrupole provides confidence that these magnets can work with minimal redesign, optimized for the Tevatron system. The C0 optics requires a gradient which is 20% lower than that of the LHC quadrupole. Independent of this, no changes in the coil design or body mechanical support are envisioned. Optimizations will focus on reducing the iron yoke diameter and overall cryostat size such that the height of the beam above the tunnel floor in the Tevatron can be accommodated without any new civil construction in the tunnel.

Changes that have been made include

- Reducing the iron yoke OD

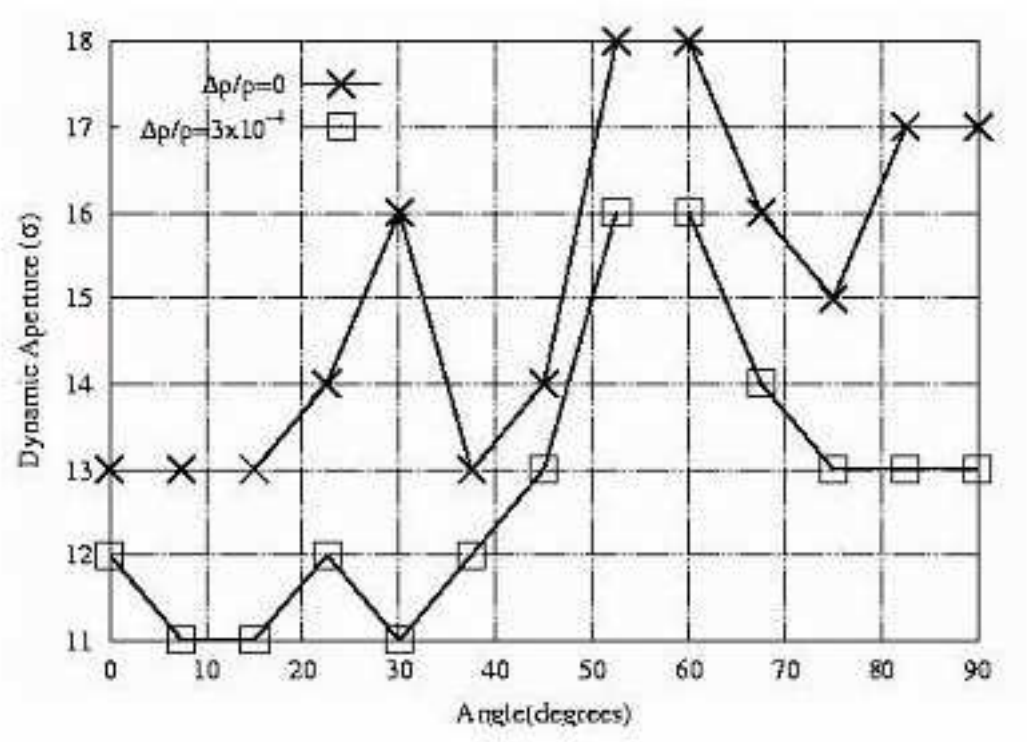

Figure 5.14: Current Run II B0/D0 Collision lattice. Single beam dynamic aperture with $\epsilon_N = 20\pi\mu$m and Δp/p = 3×10^{-4}.

- Reducing the overall magnet OD
- Changing the quadrant splice design
- Changing the expansion loop design
- Changing the pipes included and the interfaces of the cryostat
- Reducing the overall diameter of the cryostat

The redesign of the iron yoke results in a yoke OD of 311mm, and an anticipated total OD including stainless steel skin of approximately 324mm. Figure 5.19 illustrates the yoke redesign.

Given the smaller magnet, and the elimination of a superfluid helium heat exchanger required in the cryostats of the LHC Inner Triplet, the C0 quadrupole cryostats are expected to be only 1/2 the diameter of the LHC cryostats, and allow for the beam height to be located

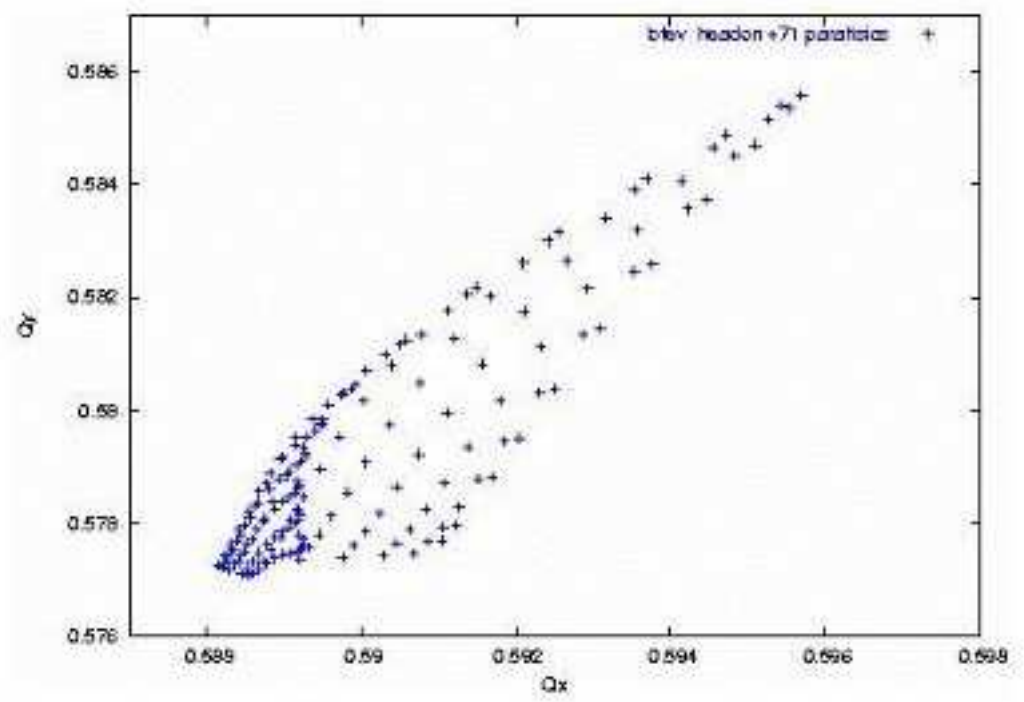

Figure 5.15: C0 collision lattice. Beam-beam effects are included for the 2 head-on collisions plus the 70 long-range interactions.

10" above the nominal Tevatron tunnel floor. The cold magnetic length of any of the Q1 to Q5 magnets is expected to be approximately 0.24m shorter than the warm mechanical length of the cold mass, end plate to end plate, as depicted in Figure 5.20. The length of the quadrant splice block, expansion loops, bus connections, instrumentation wires, and other components are included in the cryostat layouts, and at this stage appear consistent with the mechanical slot lengths listed in Table 5.16, as constrained by the lattice design. These lengths are still being optimized.

A summary of the 4.5^{o}K quench performance of the LHC model magnets and the LHC prototype magnet is shown in Figure 5.21. The magnets showed no signs of retraining. Since the C0 designs are in between these lengths, we can reasonably expect similarly good quench performance at the maximum C0 operating current of 9560A.

The iron yoke of the magnet provides flux return, and supports the stainless steel shell that provides helium containment. Since the C0 operating gradient is 20% lower than the LHC requirement, the iron yoke has been re-optimized and the outside diameter reduced

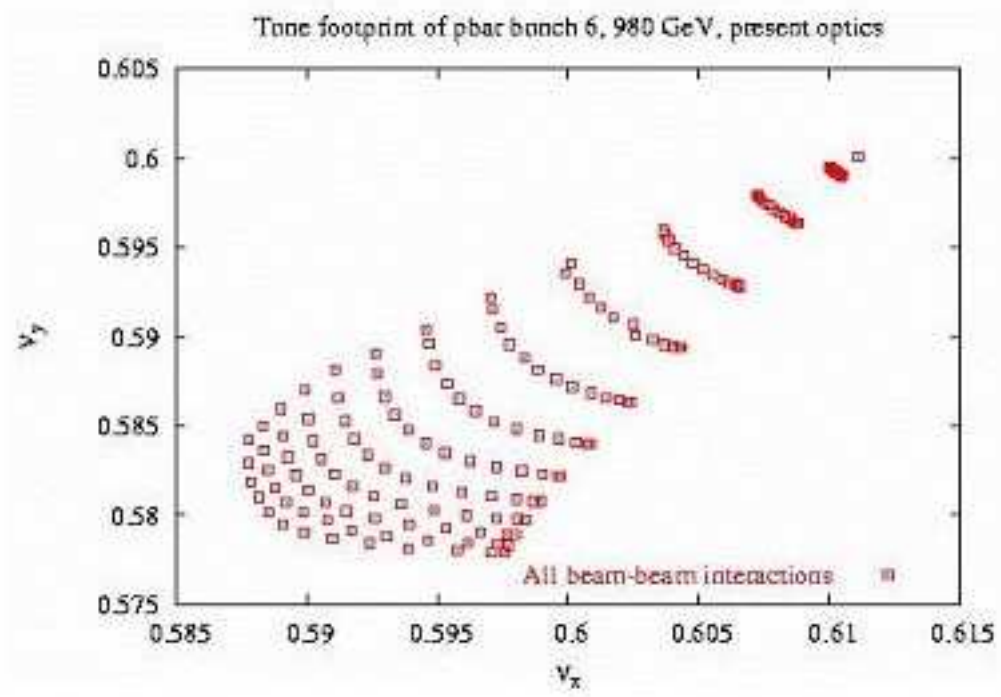

Figure 5.16: Dynamic aperture of pbar bunch #6 with beam-beam effects in the B0/D0 collision lattice.

to produce a more compact design, with acceptable harmonics. As with the LHC design, we expect to use the ICB welding press to close the skin, after it has been modified for the reduced yoke diameter.

The C0 IR quadrupole design is based on the LHC quadrupole [1] which was designed to operate at 1.9K in superfluid helium with the critical current and temperature margins necessary to operate in a large radiation induced heat load. The C0 IR quadrupole will utilize this proven design - particularly the collared coil assembly which determines the basic field properties with modifications as necessary to meet C0 specifications. One such modification is to the iron yoke, originally designed for field gradients up to 230 T/m; it must be reduced in diameter to meet the beam tube height limitations imposed by the Tevatron tunnel.

Figure 5.22 shows a concept of the completed cryostat assembly. Each magnet will be supported at 2 locations along the length, with the internal and external supports at the same location. Alignment fiducials are located on either side of the external reinforcing sections, and by using the single stretched wire measurement system the average cold magnetic axis

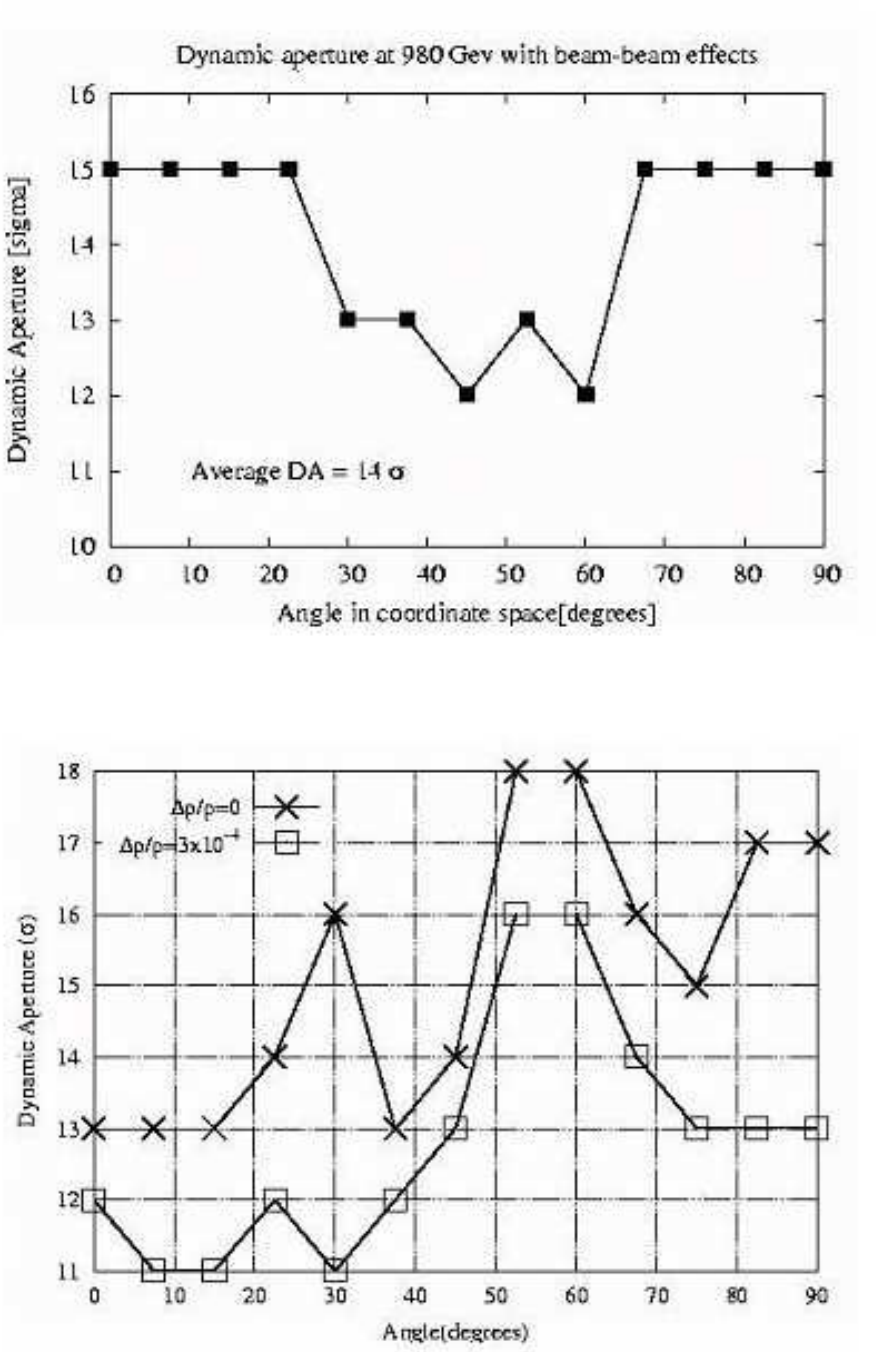

Figure 5.17: a) (upper) Current C0 collision lattice. Dynamic aperture including beam=beam effects. b) (lower) Current Run II B0/D0 Collision lattice with $\epsilon_N = 20\pi\mu$m and Δp/p = 3×10^{-4}.

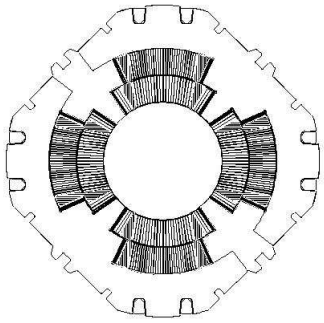

Figure 5.18: LHC Quadrupole Collared Coil.

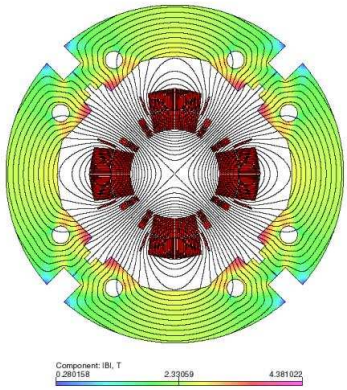

Figure 5.19: C0 IR Magnet Yoke Cross Section

can be related to these fiducials to within 200μm. Lifting of the magnet is accomplished through the use of slings in the region near the reinforcing section.

5.3.2 Corrector Design

A notable change in corrector requirements for the C0 interaction region is the addition of 'strong' quadrupole correctors with an integrated gradient of 25T-m/m. The other corrector strength requirements are comparable to existing Tevatron correctors. In addition, the new correctors do not contain octupole coils or skew sextupole coils, as do some of the original Tevatron correctors. Table 5.17 below summarizes the corrector strengths compared to existing Tevatron coils.

There are two types of corrector spools necessary for the C0 IR. The shorter spool

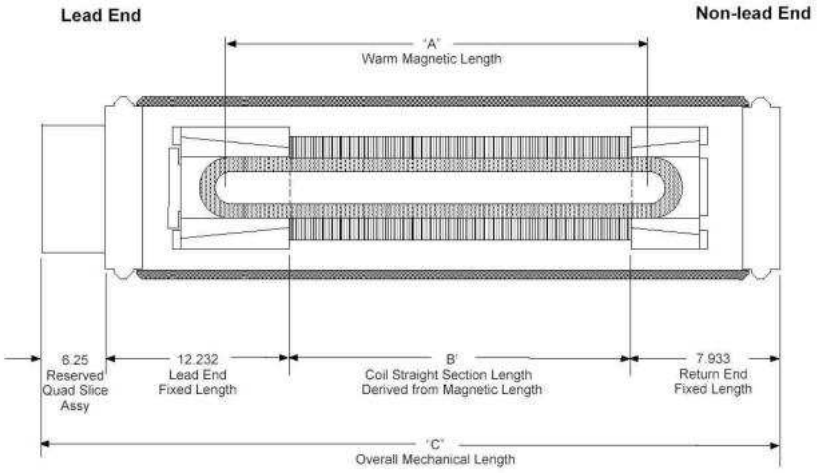

Figure 5.20: Magnetic / Mechanical Length Schematic (dimensions in inches)

Corrector type	Existing Correctors	C0 Requirements	units
dipole	.460	.480	T-m
quadrupole	7.5	7.5	T-m/m
quadrupole	none	25	T-m/m
sextupole (up)	449	450	T-m/m2
sextupole (down)	346	450	T-m/m2
octupole	30690	none	T-m/m3

Table 5.17: Corrector maximum strength comparison

("56in"=1420mm) has 800 mm available for correction elements containing both normal dipoles(ND) and skew dipoles(SD) and a skew quadrupole(SQ). The longer spool ("72in"=1830mm) has 1200 mm available for correction elements containing either normal or skew dipoles, normal quadrupoles(NQ) of 25 T-m/m maximum strength and a normal sextupole(NS) of 450 T-m/m2 maximum strength.

New correctors will be needed to meet C0 requirements. Our baseline approach uses the 'traditional' cos(nθ) design for the magnetic elements, with a separate correction element for each term. The higher order correctors are nested concentrically around the beam pipe, but the strongest lower order corrector is mounted separately. This baseline design is quite similar to correctors in the Tevatron and those being built for the LHC.

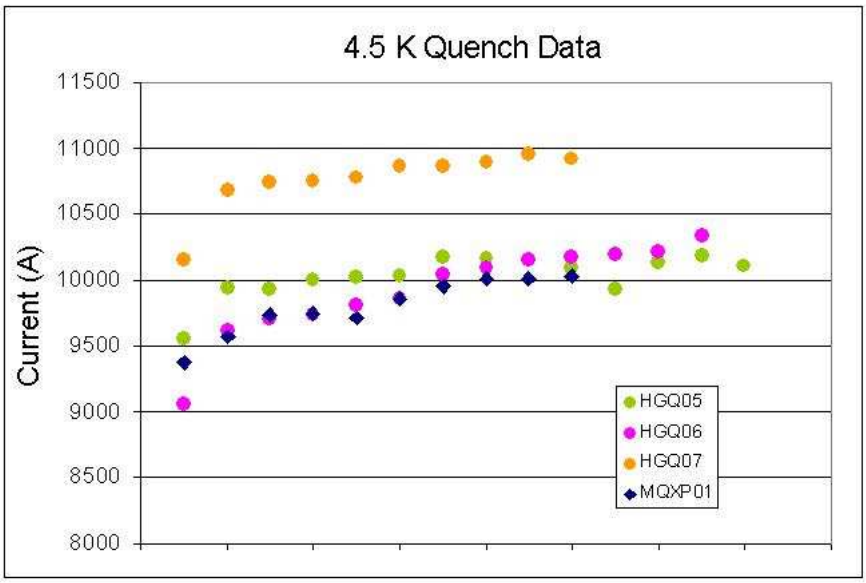

Figure 5.21: LHC Model Magnet and Prototype 4.5^{o}K Quench Performance

5.3.2.1 56" (1420mm) spool

In order to meet spatial constraints, some of the correction coils must be nested on top of others. The normal and skew dipoles are combined in one magnet assembly since they generate the same field strength and thus have similar magnetic lengths. All coils are based on the same ribbon cable with 10 strands of 0.3 mm diameter, slightly keystoned for maximum efficiency. The conductor critical current density is assumed to be that of the SSC conductor. The coil cross-sections are optimized for the best field quality achievable without wedges using the ROXIE code [2]. At this stage of optimization, the magnetic permeability of the iron yoke is taken to be constant and equal to 1000. The coil inner diameter is fixed at 80 mm. Figure 5.23 shows cross-section and the field plot in the ND/SD coils at maximum required strength in both coils. The peak field point is in the outer layer of the (inner) ND coil. The maximum field in the SD coil is 7% lower. The cross-section and field plot in the skew quadrupole coil is shown in Figure 5.24. Peak field point in this case belongs to the pole turn of the inner layer.

The parameters of the correction elements are summarized in Table 5.18. Since they are more complicated in design, the nested ND/SD coils are provided with 55-59% quench margin while the single SQ coil has 38% margin. To provide the necessary integral field strengths, the ND/SD coils have a magnetic length of 0.35 m and the SQ coil length is 0.14 m. Given reasonable assumptions for the coil end lengths, the physical lengths of ND/SD

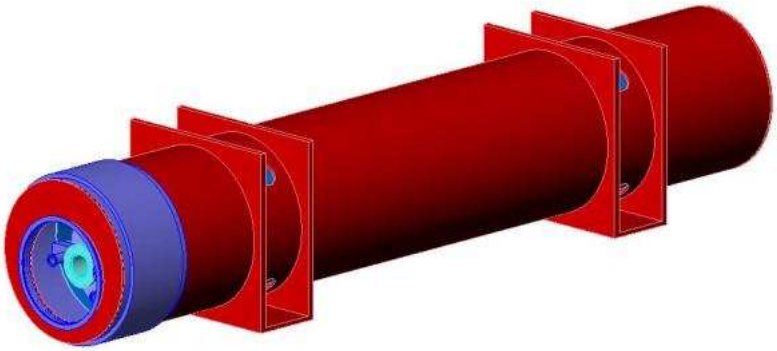

Figure 5.22: Complete Cryostat Assembly Preliminary Concept

and SQ magnets are 0.55 m and 0.25 m respectively. These lengths fill all the space available for correction elements.

5.3.2.2 72" (1830mm) spool

Similar to the 56" spool, some of the coils in the 72" spool must be nested. To reduce Lorentz forces, the normal quadrupole and sextupole coils are combined in one magnet assembly. All coils are based on the same ribbon cable used in the 56" spool. Again, the coil cross-sections are optimized for the best field quality achievable without wedges using ROXIE code; the magnetic permeability of the iron yoke is taken to be constant and equal to 1000; the coil inner diameter is fixed at 80 mm. Figure 5.25 shows the cross-section and field plot in the NQ/NS coils at the nominal current. The peak field point is in the inner layer of the (inner) NQ coil. The maximum field in the NS coil is 6% lower. The cross-section and field plots for the normal dipole coil is shown in Figure 5.26. Peak field point in this case is in the pole turn of the inner layer.

Parameters of the correction elements are summarized in Table 5.19. The nested NQ/NS coils have 41-43% quench margin while the single ND coil has 39% margin. To provide the necessary integral field strengths, the NQ/NS coils will have magnetic lengths of 0.68 to 0.70 m and the ND coil of 0.20 m. Given reasonable assumptions on the coil end lengths, the

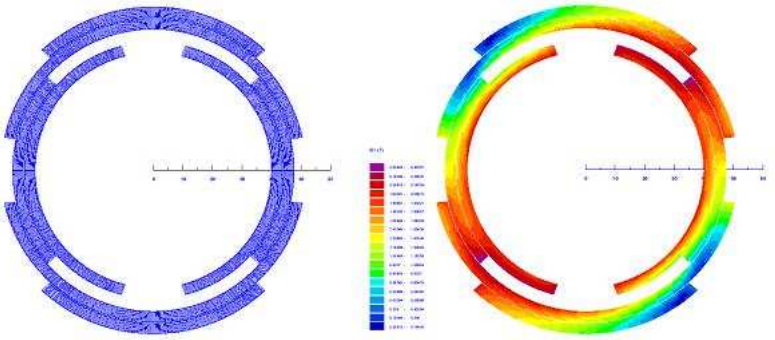

Figure 5.23: ND/SD coil cross-section (left) and field distribution (right).

Parameter	Unit	ND	SD	SQ
n		0	0	1
Coil IR	mm	40.0	48.0	40.0
Yoke IR	mm	60.0		53.0
Strands/cable		10		
Bare strand diameter	mm	0.300		
Cu/nonCu ratio		2.0		
J_{nonCu}(5T, 4.2K)	A/mm^2	2750		
Maximum strength required	Tm/mn	0.48	0.48	7.5
Current maximum strength	A	27.2	23.6	49.0
Quench margin at nominal current in all the coils	%	54.7	58.8	38.2
Inductance	H/m	15.16	25.03	6.48
Stored energy at I_{nom}	kJ/m	5.61	6.97	7.78
Magnetic length	m	0.350	0.351	0.143
Physical length	m	0.55		0.25

Table 5.18: 56" spool corrector parameters.

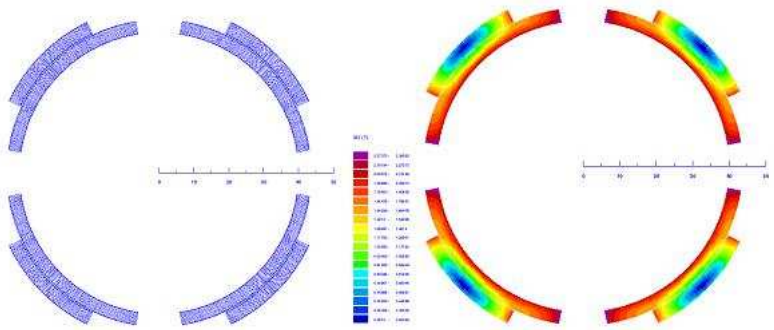

Figure 5.24: SQ coil cross-section (left) and field distribution (right).

physical lengths of NQ/NS and ND magnets are 0.8 m and 0.4 m respectively. This utilizes all the space available for correction elements.

5.3.3 Support Systems

We describe briefly the subsystems required to support the operation of the magnets that comprise the C0 Interaction Region. Many more details are available elsewhere [1].

5.3.3.1 HTS (High Temperature Superconducting) Leads

The 10kA current leads for the high gradient quadrupoles in the C0 IR will be made from high temperature superconductor (HTS) to avoid additional loading of the 4.5^{o}K He system. In the present Tevatron configuration, four spool pieces have been modified to incorporate 5kA HTS leads, and one of these has been installed in the ring for several years. The cost and time scale associated with development of new, optimized 10kA HTS leads does not fit within BTeV constraints, so we have adopted a baseline configuration in which the 10kA power leads are composed of pairs of the existing 5kA design. The drawbacks of this approach are obvious – it doubles the number of lead assemblies, associated piping, instrumentation, and space allotment. An alternative is that the single 5kA HTS leads may, with increased

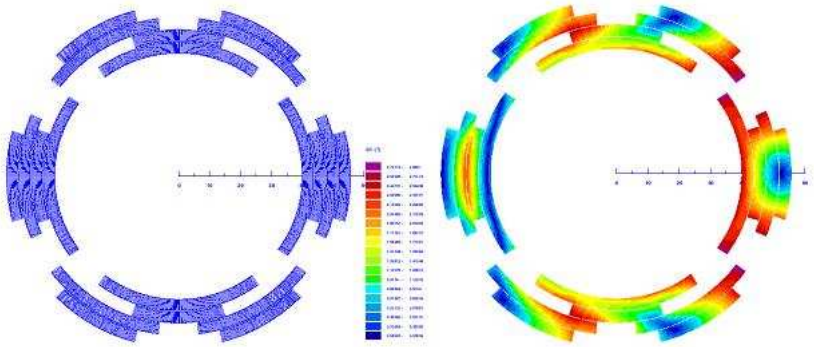

Figure 5.25: NQ/NS coil cross-section (left) and field distribution (right).

Parameter	Unit	NQ	NS	ND
n		1	2	0
Coil IR	mm	40.0	48.0	40.0
Yoke IR	mm	60.0		53.0
Strands/cable		10		
Bare strand diameter	mm	0.300		
Cu/nonCu ratio		2.0		
JnonCu(5T, 4.2K)	A/mm2	2750		
Maximum required strength	Tm/mn	25	450	0.48
Current maximum strength	A	40.0	36.6	43.0
Quench margin at nominal current in all the coils	%	40.6	42.9	39.2
Inductance	H/m	5.42	6.24	17.01
Stored energy at Inom	kJ/m	4.34	4.18	15.73
Magnetic length	m	0.676	0.696	0.200
Physical length	m	0.8		0.4

Table 5.19: 72" spool corrector parameters

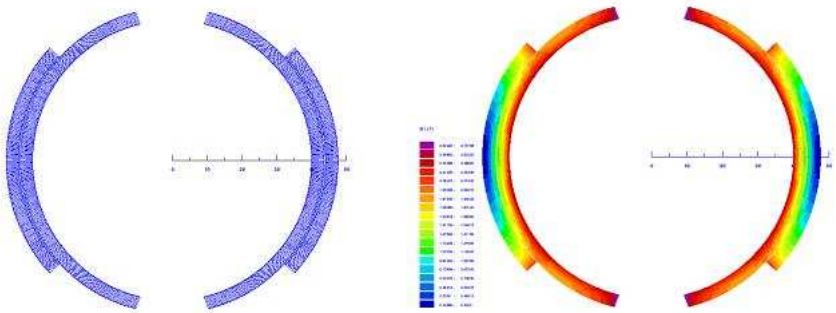

Figure 5.26: ND coil cross-section (left) and field distribution (right).

coolant flow, be able to carry currents approaching 10,000 Amps. Tests are underway to investigate the electrical and thermal stability of these leads.

5.3.3.2 Power Supplies and Bus work

The low beta quadrupole power supplies for the C0 interaction region will be located in the B4, C0, and C1 service buildings. There are 10,000 Amp and 5000 Amp supplies, along with some lower current supplies. The 10,000 Amp supplies are obtained by running two 5,000 Amp supplies in series.

Bus work to and from the magnet loads is the main resistive loss in the system and will drive the power supply voltage. The correct amount of copper to use in the bus work is such that the installation cost is equal to the power bill for running the system for a set period of time (like five years). As with the Main Injector, this works out to be on the order of 4 square inches of copper bus per 5,000 A RMS of current. For the 10,000 A runs the plan is to install two 4 square inch runs in parallel for supply and return.

5.3.3.3 Corrector Power Supplies

The independent corrector power supplies required for the C0 IR are detailed in the full C0 CDR. For B4 and C1 sectors, the count of independent channels goes from 22 for Run II to

35 for the C0 IR. The B4 and C1 service building corrector power supply installations will be maintained as is and the additional 13 channels will be located in C0 with a new bulk supply and individual switch mode, four-quadrant power supplies providing the regulation off of the bulk supply. The proposed supplies are a very mature design and is a virtual copy of the Main Injector system which is barely 5 years old.

5.3.3.4 Cryogenics

The C0 low beta cryogenic components are cooled by a hybrid cryogenic system that consists of the C1 and B4 satellite refrigerators, and the Central Helium Liquefier (CHL). The heat load of the magnets, static and dynamic, is removed by the single-phase, and then is absorbed by the latent heat of vaporization of the two-phase helium. The single-phase helium is also used to cool correction, safety, power and crossover leads. To lower the operating temperature of the magnets, a single stage cold compressor is used in each house. The total load on the cryogenic system is comprised of the magnet string's static and dynamic heat load, lead flows, and cold compressor heat of compression.

5.3.3.5 Vacuum

Even though 95% of the Tevatron total length is cryogenic, poor vacuum in warm sections of the Tevatron is currently the major source of beam halo background in the collider detectors at B0 and D0. Generally the vacuum requirement for the Tevatron warm straight sections is an absolute pressure of 1×10^{-9} Torr. This should be used as an operational goal for warm vacuum sections which do not contain electrostatic separators. Individual components should be designed for better than that, perhaps 3-5$\times10^{-10}$ Torr, if this can be achieved by reasonable means such as hydrogen degassing, electropolishing and baking.

The vacuum requirement for warm sections which contain electrostatic separators is more stringent. The operational goal is 5×10^{-11} Torr.

The vacuum in the BTeV detector itself may be poorer, with pressures on the order of 1×10^{-8} Torr being discussed as an operational goal. Gas load migrating from this region into the Tevatron regions will be mitigated by 50 l/sec ion pumps located near the boundaries of this region.

5.3.3.6 Modification to QPM System and Controls

Only minor modifications to the QPMs at B4 and C1 are required. No major new controls software is required, but minor modifications to a large suite of programs, and some duplication of existing software will be necessary. A significant number of database entries will also need to be made for new power supplies, separators, vacuum devices, etc.

5.3.3.7 Instrumentation

There are currently 12 Beam Loss Monitors (BLM) located in each of the B4 and C1 houses. This number is adequate for the C0 IR. They will be repositioned in the tunnel for optimum

utility. There are currently 19 Beam Position Monitors (BPM) located in the B4 and C1 houses. For the C0 IR this number will be increased to 29.

Tiltmeters similar to what currently exist on the B0 and D0 low beta quadrupoles will be installed on the C0 low beta quadrupoles. This is an essential piece of instrumentation because the Tevatron orbit and coupling are very sensitive to motion of these quadrupoles due to the large β functions. Unlike on the B0 and D0 low beta quads, robust mounting and alignment of these tiltmeters will be designed into the cryostat housing of the C0 low beta quads.

5.3.3.8 Separators

Six separators, identical to previously built separators, are required. There will be 2 horizontal and 1 vertical separator at B49 and 2 vertical and 1 horizontal separator at C11. These separators are delicate, and special handling equipment and false floors must be provided to install them.

5.3.3.9 Shielding

Concrete shielding walls at the upstream and downstream ends of the C0 collision hall will be of a clamshell design and on rollers, so they can be easily moved when changing a magnet in the area.

5.3.3.10 Collimators

Two new collimators, of standard design, will be installed in a 2.6 meter warm straight section near B47-4.

5.4 A History of Other Approaches to Design of the Interaction Region

There have been several attempts to design an interaction region at C0, starting in 1996.

The earliest attempts centered on achieving relatively low luminosity goals mainly to enable the use of C0 as an area for carrying out detector R&D. These attempts had to preserve the luminosity at B0 and D0 for the two collider experiments. One attempt required the use of spare magnets with no construction of new components. Although significant effort was expended on looking for solutions, no satisfactory design was ever developed.

When the BTeV proposal was being developed in 1999 and 2000, work was started on a custom IR capable of producing the high luminosity, 2×10^{32}, that was needed. A successful design was achieved based on use of modified LHC low beta quadrupoles. This design produced a β^* of 50 cm, which would give C0 70% of the luminosity at B0 or D0. Given the luminosity goals of that time, this produced adequate luminosity for BTeV. An external review of this design was conducted in 2001 and the design was pronounced sound but the

review committee specified additional studies before it could be certain that it would work. At about this time, personnel were moved off the project onto other, higher priority activities.

In early 2002, after a subpanel of HEPAP had cited budgetary concerns about BTeV, BTeV was rescoped to reduce its cost. One part of the rescoping involved creating the IR by taking magnets from either B0 or D0, or both, and deploying them in C0. The design that was produced resulted in a β^* of around 1.0 m. This resulted in a luminosity that was about 0.3 of that in B0 and D0. Again, with optimistic assumptions about the ultimate luminosity achievable in Run 2, this resulted in a luminosity at C0 that was close to BTeV's design luminosity. At the same time, the BTeV detector was also descoped.

In September of 2003, the P5 subpanel of HEPAP endorsed the descoped BTeV detector, and recommended the construction of the custom IR. The IR design effort was restarted and resulted in the design described here and in Ref. [1]. This design resulted in a β^* of 35cm, which gives C0 the same luminosity as B0 and D0.

The long path taken to the current design has led to an evaluation of many approaches and investigations of availability of suitable magnets at Fermilab and at other accelerator labs. The current design represents the evaluation of many alternatives and is the optimal result given the constraints and requirements described in the introduction to this section.

Bibliography

[1] full CDR

[2] ROXIE Code, Vector Fields, Inc., Illinois, 60505, USA.